System Level Modeling of Thermal Transients in PEMFC Systems

Bryan W. Shevock

Thesis submitted to the faculty of the Virginia Polytechnic and State University in partial fulfillment of the requirements for the degree of

Master of Science
In
Mechanical Engineering

Committee:

Dr. Douglas Nelson, Chairman
Dr. Michael Ellis
Dr. Michael von Spakovsky

January 28, 2008
Blacksburg, Virginia

Keywords: Fuel Cell, Hydrogen, Polymer Electrolyte Membrane, PEM, PEMFC, System Modeling, Simulink

System Level Modeling of Thermal Transients in PEMFC Systems

Bryan W. Shevock

Abstract

Fuel cell system models are key tools for automotive fuel cell system engineers to properly size components to meet design parameters without compromising efficiency by over-sizing parasitic components. A transient fuel cell system level model is being developed that includes a simplified transient thermal and parasitics model. Model validation is achieved using a small 1.2 kW fuel cell system, due to its availability. While this is a relatively small stack compared to a full size automotive stack, the power, general thermal behavior, and compressor parasitics portions of the model can be scaled to any number of cells with any size membrane area. With flexibility in membrane size and cell numbers, this model can be easily scaled to match full automotive stacks of any size.

The electrical model employs a generalized polarization curve to approximate system performance and efficiency parameters needed for the other components of the model. General parameters of a stack's individual cells must be known to scale the stack model. These parameters are usually known by the time system level design begins. The thermal model relies on a lumped capacity approximation of an individual cell system with convective cooling. From the thermal parameters calculated by the model, a designer can effectively size thermal components to remove stack thermal loads.

The transient thermal model was found to match experimental data well. The steady state and transient sections of the curve have good agreement during warm up and cool down cycles.

In all, the model provides a useful tool for system level engineers in the early stages of stack system development. The flexibility of this model will be critical for providing engineers with the ability to look at possible solutions for their fuel cell power requirements.

Acknowledgements

I would like to thank Dr. Nelson for his support through this project and guidance throughout my college career.

I would also like to thank my parents, George and Debbie Shevock, for their faith in me and always pushing me to be better.

Table of Contents

List of Multimedia Objects

Tables

Figures

Equations

Abbreviations

PEMFC	Proton Exchange Membrane Fuel Cell
ICE	Internal Combustion Engine
GDL	Gas Diffusion Layer
MEA	Membrane Electrolyte Assembly
V_{cell}	Single cell voltage
V_{oc}	Open circuit voltage
J	Current density
R	Stack resistance
$R_{per\ T}$	Change in stack resistance with T
T_{stack}	Stack temperature
Tref	Reference temperature
V_{stack}	Stack voltage
N_{cells}	Number of cells in the stack
$\dot{N}_{e-}$	Molar flow rate of electrons
I_{gross}	Gross stack current
$(\dot{m}_{H_2})_{react}$	Mass flow rate of reacting hydrogen
MM_{H_2}	Molar mass of hydrogen
$(\dot{m}_{O_2})_{react}$	Mass flow rate of reacting oxygen
MM_{O_2}	Molar mass of oxygen
$(\dot{m}_{H_2O})_{gen}$	Mass rate of water generation
$(\dot{m}_{O_2})_{in}$	Mass flow rate of oxygen into stack
SR_{O_2}	Stoichiometric ratio oxygen
$(\dot{m}_{H_2})_{in}$	Mass flow rate of hydrogen
SR_{H_2}	Stoichiometric ratio of hydrogen
$(\dot{m}_{air})_{in}$	Mass flow rate of air
MM_{air}	Molar mass of air
$(\dot{m}_{N_2})_{sys}$	Mass flow rate of nitrogen
MM_{N_2}	Molar mass of nitrogen
$(\dot{m}_{H_2O})_{in}$	Mass flow rate of water
ω_{amb}	Ambient humidity ratio
$(\dot{m}_{H_2O})_{out}$	Mass flow rate of water out
P_{stack}	Stack power
P_{fuel}	Fuel power
LHV_{H_2}	Lower heating value of hydrogen
$\dot{Q}_{gen}$	Rate of heat generation
ε_{stack}	Stack efficiency
$\dot{m}_{H_2O(l)}$	Mass flow rate of liquid water
$\dot{m}_{H_2O(v)}$	Mass flow rate of water vapor

MM_{H_2O}	Molar mass of water
$P_{H_2O(v)}$	Partial pressure of water vapor
P_{amb}	Ambient pressure
m_{cell}	Cell mass
c_{cell}	Cell specific heat
Cp	Specific heat
D_h	Hydraulic diameter
A_c	Cooling channel cross section area
P	Cooling channel perimeter
Re	Reynolds number
ρ	Density
$\bar{u}_m$	Cooling air average velocity
μ	Viscosity
f	Friction factor
q	Rate of heat rejection
q_t	Rate of heat rejection from fin array
$\bar{h}$	Convection heat transfer coefficient
k	Thermal conductivity
η_0	Fin efficiency
$\theta_{b,lm}$	Log mean temperature difference
h	Cooling channel height
w	Cooling channel width
l	Cooling channel length
ω_{ex}	Exhaust humidity ratio
ε	Humidity exchanger efficiency
D_{comp}	Compressor outlet diameter
D_h	Hydraulic diameter of one cooling channel
$\varepsilon_{el,comp}$	Compressor electrical efficiency

1. Introduction

There are many types of fuel cells in development and in practical applications today. This paper will focus on proton exchange membrane fuel cells (PEMFC). PEMFCs are the primary type of fuel cells currently under development for the automotive industry. This is due to the relatively quick startup times and high power density compared with other fuel cell technologies.

The first step to mathematical modeling is to have a good understanding of the physical system. To do this, three key introductory questions must be asked. They are, "What is a fuel cell?", "How do they work?", and "What are they used for?".

1.1 What is a Fuel Cell

A fuel cell is a device that utilizes an electrochemical reaction to generate electricity from a fuel. In the case of PEMFCs, this fuel is gaseous hydrogen. Like internal combustion engines (ICE) oxygen is also required for the reaction. In most applications, ambient air is used as the oxygen source. The basic building block of a fuel cell is called a cell. Since the open circuit output voltage of a cell is only approximately one volt, several cells are stacked together to create a fuel cell stack. In automotive applications, it is common for a stack to be made of 200-300 cells or more.

1.2 How do Fuel Cells Work

As mentioned, fuel cells utilize an electrochemical reaction to generate electricity. To support this electrochemical reaction, a substructure called a cell was developed. These cells are put together in a structure known as a fuel cell stack.

1.2.1 Cell Structure. Like other fuel cells, the basic element of a PEMFC is a cell. The cell consists of four major structures including electron collection plates, gas diffusion layers (GDL), a catalyst coated electrolyte membrane, and a closed electrical circuit between the two collection plates. The actual assembly of these structures is shown in Figure 1. Hydrogen is supplied to the cell through channels in the collection plate on the anode side of the electrolyte membrane. It then diffuses through the GDL to the surface of the electrolyte membrane where the first half of the electrochemical reaction occurs. As the name suggests, one of the GDL's purpose is to assist gas diffusion across the entire surface of the catalyst layer on the electrolyte membrane. This diffusion principle is further illustrated in Figure 2. Without the GDL, the only areas of the membrane surface where reactions could occur would be those areas in direct contact with the reactant gas flow channels, and there would be no conductor present to carry electrons away from the reaction sites. This is a waste of expensive membrane and catalyst materials.

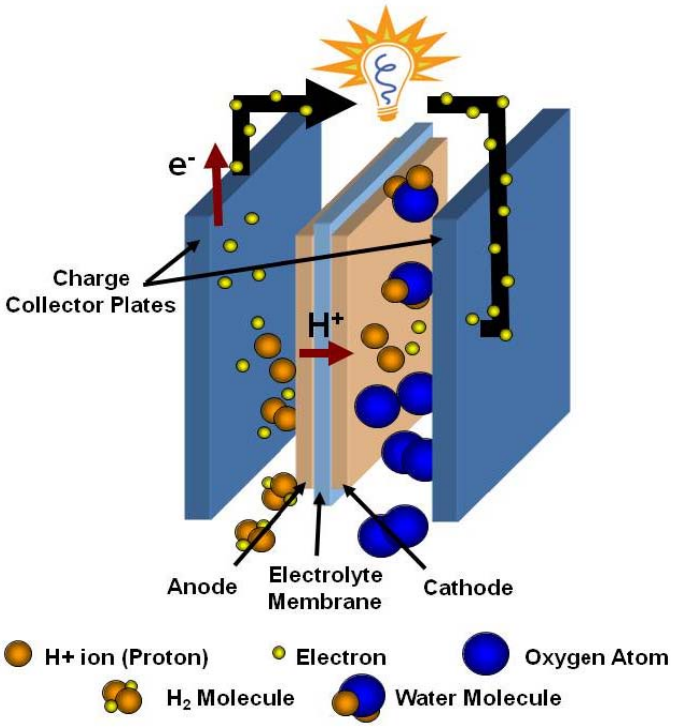

Figure 1. The basic structure of a cell showing the path of the electrochemical reaction

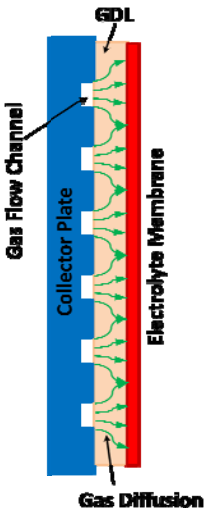

Figure 2. The GDL allows for gas to reach the entire surface of the membrane

The electrolyte membrane is made from a polymer material that has charge sites for proton transport. This is generally accomplished by adding sulfonic acid functional groups to existing polymers. For example, the most widely used electrolyte membrane in PEMFCs is known by the trade name Nafion®. Nafion® has the same backbone structure as Teflon® but has added sulfonic acid groups [1]. Without significant amounts of water in the membrane, Nafion's® ion conductance significantly diminishes. Much of the water needed to maintain ion conductance

comes from the cathode reaction. Many systems utilize reactant gas humidification to maintain membrane hydration.

Similar to the anode, oxygen or air flow through channels in the collection plate on the cathode side of the electrolyte membrane. The oxygen also flows through a GDL to help increase the active surface area of the electrolyte membrane surface. The cathode is where the second half of the electrochemical reaction occurs and where the product water is created. The product water is removed from the cell through the same channels in the cathode collection plate that supplies the cell with oxygen.

1.2.2 The Electrochemical Reaction. As mentioned, the electrochemical reaction in a PEMFC occurs in two stages at two different locations inside of the cell. The first stage of the reaction occurs at the anode. Here, hydrogen is brought into the cell through the flow channels and it diffuses through the GDL to the catalyst layer on the electrolyte membrane. The first half of the electrochemical reaction takes place were there is material from the electrolyte membrane (proton conductor), catalyst, GDL (electron conductor), and hydrogen present in one area at the microscopic level. Here, the catalyst breaks the hydrogen molecules into hydrogen ions (protons) and electrons. The chemical reaction can be written as

$$H_2 \rightarrow 2H^+ + 2e^-. \tag{1.1}$$

The hydrogen ions pass through the electrolyte membrane which is conductive to protons but not electrons. Since the electrons cannot pass through the membrane, they are carried away from the reaction site through the electrically conductive GDL, into the anode collector plate and then through an electric circuit.

The hydrogen ions pass through the electrolyte membrane to the cathode. Here they are met by the electrons from the electric circuit connected to the anode and oxygen gas. A catalyst combines the oxygen, hydrogen ions, and electrons into water molecules which exit the cell as exhaust through the flow channels in the cathode collector plate. This reaction can be written as

$$2H^+ + e^- + \frac{1}{2}O_2 \rightarrow H_2O. \tag{1.2}$$

Combining equations 1.1 and 1.2 gives the overall reaction of the fuel cell and can be written as

$$H_2 + \frac{1}{2}O_2 \rightarrow H_2O. \tag{1.3}$$

A good illustration of the reactant gas, ion, and electron flows is found back in Figure 1.

From equation 1.3, one of the key advantages of fuel cells is easily seen. This is that the only product of the reaction is water which is far better for the environment than the harmful products of combustion in a gasoline or diesel ICE.

1.2.3 Stack Construction. Since the open circuit output voltage of one cell is approximately one volt and effective voltage with the stack under load is 0.5 to 0.6 volts, several cells are typically arranged in series to boost the output voltage. Cells are stacked side by side and the cathode collector plate from one cell becomes the anode collector plate for another cell. In doing this, one single plate becomes the high electrical potential plate for one cell and the low potential plate for the adjacent cell. Because of this dual polarity of the collector plates, they are called bi-polar plates in a stack application. A typical stack configuration is illustrated in Figure 3. An automobile application may require 300 cells in a stack to meet voltage and power requirements while a cell phone application may require as few as 1-5 cells.

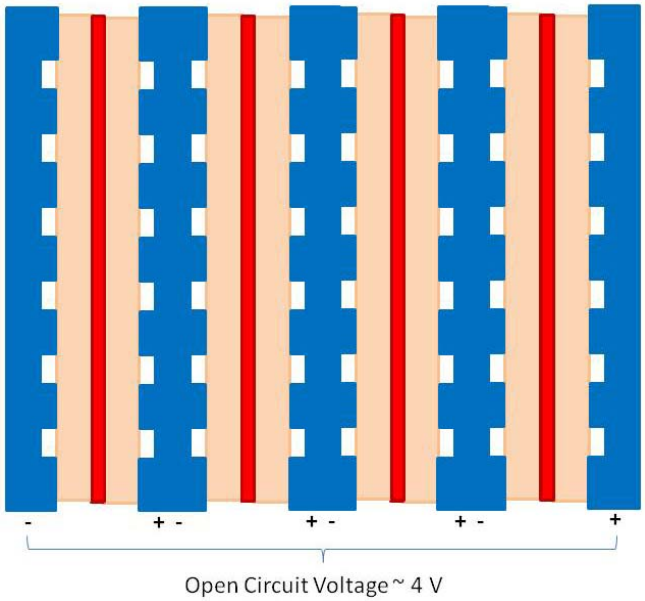

Figure 3. Typical stack configuration with bi-polar plates

1.2.4 Support Systems. There are several key systems that a fuel cell must have in order to maintain normal operations. These include fuel systems, reactant air/oxygen systems, humidification systems, and cooling systems.

Fuel systems can either be the most simplistic system or the most complex system needed. In the case of pressurized hydrogen storage, the fuel system typically consists of pressurized hydrogen storage tanks and a series of regulators to bring the fuel pressure down to levels that will not tear the membrane electrolyte assembly (MEA) which consists of everything between the bi-polar plates. If the fuel cell system is utilizing fuel reformers to generate the hydrogen used in the stack, the system gets much more complicated and expensive. Other means of hydrogen storage

are undergoing research. The US Department of Energy is currently looking at advanced metal hydrides, high surface area sorbents, and chemical storage among others as potential storage solutions [2]. Each of these systems increases the complexity of the fuel system.

Most fuel cells use air as the oxidant for the reaction. In these cases, air is drawn from the atmosphere and compressed by an electric compressor before entering the stack. Pressurization increases the performance of the fuel cell due to there being more oxygen available to the reaction. While pressurizing the cathode air increases performance, it also is a source of parasitic losses. The compressor requires electricity that the fuel cell generated in order to compress the air. This decreases the amount of net power the system can generate. There is a balance between performance increases and parasitic losses in the cathode air supply system. This is one reason mathematical modeling of these systems is critical for their optimization.

The electrolyte membranes used in PEMFC stacks require significant membrane hydration to maintain their proton conductivity. Smaller stacks, like the Ballard Nexa® used in the validation of this model, simply use humidity exchangers between the cathode exhaust and stack inlet to ensure the oxidant air is moist as it enters the stack. These humidity exchangers work similarly to heat exchangers except that instead of transferring heat, moisture is transferred through a water permeable membrane. On the other hand, larger automotive style stacks can have much more complex humidification systems. Many humidify the incoming hydrogen as well as the oxidant air to ensure the membrane remains moist through its entire thickness. The need for significant water content in the membrane for proton conductivity brings about one of the major shortfalls of PEMFC systems especially in the automotive industry. Vehicles are routinely subjected to sub freezing temperatures. The US Department of Energy has conducted tests to characterize Nafion's® ion conductivity in extreme cold temperatures. The findings were that with water hydrated stacks, Nafion's® conductivity drops off faster in sub-freezing temperatures than it does in above freezing temperatures [3]. This significantly reduces the performance of a fuel cell in these extreme conditions. In fact, cold temperatures have been known to significantly reduce the life of a fuel cell [3]. Cold starts are one of the key items that automotive stack designers are trying to address. Transient thermal models such as the one outlined in this paper are useful for understanding and optimizing stack warm-up to both protect the membranes and provide the power that is required to power a vehicle in extreme conditions.

At peak efficiency, the best fuel cell stacks operate at approximately 60% efficiency. This means that approximately 40% of the energy that enters the stack through the hydrogen fuel is generated into heat that must be carried away from the stack. Currently, there are two primary means for cooling stacks. They are air cooling and water cooling. Air cooling a stack requires much more volume for the cooling channels. Therefore, this cooling method is generally used for smaller stacks whose energy density requirements are low such as the Ballard Nexa® system. Additionally, the parasitic losses associated with air cooled stacks can be larger at high cooling

loads due to the inherent inefficiency of blowing air through channels at higher velocities. For these reasons, water cooling dominates the automotive fuel cell market. These stacks can be made smaller due to smaller cooling channels, and water cooled systems seem to maintain a more constant temperature throughout the stack making the stack more predictable and consistent. Additionally, the large surface area radiators needed to dissipate heat to the ambient air can be placed anywhere giving greater packaging flexibility.

1.3 What are they Used for

The final question that needs to be answered to have a basic understanding of fuel cells is, "What are they used for?" This question needs to be looked at in two parts. They are the current uses for fuel cells and future uses for them.

1.3.1 Current Uses. The biggest push for fuel cells has come from the automotive industry in light of rapidly rising gasoline prices, a growing instability in some oil producing countries, and a growing concern for the environment. Currently, several automotive manufacturers have fuel cell fleets in service in several parts of the country. Ford released a fleet of 30 fuel cell vehicles that were delivered to five different cities in 2005[4]. General Motors responded in force by releasing a fleet of more than 100 Chevrolet Equinox fuel cell vehicles starting in 2007[5]. General Motors has also committed to demonstrating consumer feasibility of fuel cell vehicles by 2010.

While the automotive industry is currently providing the push for fuel cell development, it was NASA who pioneered one of the first major applications of fuel cells with the Apollo program. NASA needed a reliable method for producing electricity on board the space capsule and no battery was capable of storing enough charge to make it to the moon and back. There was already hydrogen and oxygen on board to fuel the rocket engines, so the logical choice was a fuel cell. NASA utilized an alkaline fuel cell to provide all electrical power to the capsule as well as a supply of water to the crew [6]. The fuel cell is still utilized for the same function on today's space shuttle.

1.3.2 Future Uses. The future potential for fuel cells is potentially endless ranging from automobiles that produce nothing but a plume of water vapor as their exhaust to cell phones that have small refillable fuel cartridges. Some envision our homes being powered by clean fuel cells while using waste heat to heat the home in the winter or for hot water. Many envision hydrogen fuel cells becoming the primary energy source for the entire country in what has been termed the "hydrogen economy". Only time will tell the extent to which fuel cells will play a role in our every day lives.

1.4 Hydrogen as a Fuel

In many ways, hydrogen has a poor public perception in that it is commonly related to the Hindenburg tragedy and nuclear fusion weapons sometimes referred to as "hydrogen bombs". The reality is that hydrogen is a safer fuel than gasoline in many ways. Hydrogen is the lightest of all of the elements and, therefore, is very diffuse in air. This means that in the event of a leak, the escaped hydrogen will often diffuse into the air and not reach a flammable state. On the other hand, gasoline will pool and the vapors can be very explosive. Today's pressurized hydrogen storage vessels are designed to release hydrogen safely through pressure relief valves away from the vehicle in the case of a thermal event. It is easy to imagine the consequences of such a test in a gasoline vehicle.

Aside from safety, hydrogen provides several other key benefits. First, the products of both its electrochemical reaction and its combustion reaction are water. There is no carbon dioxide generated in that there is no carbon in the fuel. However, as in a gasoline ICE, a hydrogen ICE has the potential to generate harmful oxides of nitrogen. In addition to its environmental benefits, there are political benefits as well. Hydrogen provides a means of meeting our energy needs without the need for foreign oil due to its ability to be generated using domestic, renewable sources of energy. Not only is much of the world's oil located in politically unstable areas, it is also a diminishing natural resource that is seeing more and more demand from developing countries. These increases in demand and the finite supply are driving energy costs up every year.

While hydrogen provides many benefits, there are also several obstacles that must be overcome as well. First, hydrogen should be characterized as an energy transporter rather than a fuel source. In other words, hydrogen must be made from other energy sources. The good news is that the energy sources that make hydrogen can be renewable sources such as solar and wind. There are also several other processes that are being researched to produce hydrogen such as biological and nuclear production although none have clearly become the front runner. In early hydrogen applications, it will most likely be reformed from natural gas. This is the current method for producing hydrogen for industrial and other uses.

Another key problem is that the most common form of hydrogen is a very light, diffuse gas. This means that while hydrogen carries more energy by mass than gasoline or any other hydrocarbon, it contains far less energy than these liquid fuels by volume. In other words, a very large volume of hydrogen must be carried on board a vehicle where space is already at a premium. Currently, pressurized storage tanks that store the gas at up to 10,000 psi (700 bar) are being used in development vehicles. This challenge is why hydrogen storage is a top project in

the research community and, as mentioned previously, the United States Department of Energy is pursuing several options [2].

Lack of infrastructure is another hurdle that must be overcome. There are very few hydrogen refueling stations in the country. As of the end of 2007, California has 25 operational hydrogen refueling stations with ten more planned [7]. These are located primarily in Southern California and the San Francisco Bay area. While these are a step in the right direction, a move to a hydrogen dominated automotive sector would be a significant investment in infrastructure.

1.5 The Importance of Modeling

Mathematical modeling provides a key benefit to a fuel cell designer. It allows for the proper system components to be designed and built in parallel without other stack hardware being in place. The cost savings is tremendous considering the cost of trial and error solutions especially considering the high cost of fuel cell hardware in general. Mathematical modeling gives designers the necessary tools to understand how the full stack system will operate without having a piece of hardware in front of them. Models are also useful when limited hardware is available and a designer needs to better understand how a stack will behave in conditions that may damage a fuel cell. For example, automotive stacks have to be able to survive below freezing ambient temperatures on cold starts. In this case a transient thermal model such as the one illustrated in this paper is critical for understanding stack behavior under these conditions.

1.6 Research Objectives

The objectives of this research are to develop and validate a transient, system-level model in Matlab/Simulink to characterize an air-cooled PEMFC stack. This model will be complete with stack power, air-cooling system, air humidification system, and parasitic loss models, and will be scalable to any number of cells or cell area in the stack. The model will focus on stack thermal transients to better understand how the stack will react in conditions such as extreme heat and extreme cold starts. Due to available validation hardware, the model will be limited to an air cooled system. Validation will be done using an instrumented 1.2 kW Ballard Nexa fuel cell system.

Once the model is fully validated, it will be used to analyze extreme stack operating conditions that would be difficult to reproduce in hardware testing or that would risk damaging the stack.

2. Literature Review

Mathematical fuel cell modeling is a hot topic in the research sector. Most fuel cell research that is currently being conducted is focused towards solving the problems that are keeping fuel cell systems out of consumer's hands such as cost, life, and extreme weather operation. Each of these challenges requires a deeper understanding of how fuel cells work and mathematical models provide a great way to experiment with several different hardware configurations without having to invest the huge amounts of money into the hardware itself. This section of the paper contains a brief summary on mathematical modeling in the literature.

2.1 Detailed Electrochemical Modeling

In 2004, Baschuk and Li [8] presented a detailed transient electrochemical model for a single cell. The model includes detailed reaction site specific electrochemical reaction equations, proton migration equations, and detailed mass transport equations for the gaseous products and reactants and the liquid product water. These equations are applied to each section of the cell including the bi-polar plates, gas flow channels, electrode backing, catalyst, and polymer electrolyte layers. The difference between this proposed model and previous works is that this model considers all three phases of matter (solid, liquid, and gas) to be present in a cell. This is also among the first models to include extremely detailed equations for mass transport, proton migration, and the electrochemical reactions into one comprehensive model. Previous models either focused on a single aspect of the cell or did not carry out the equations to this level of detail.

The model presented in this paper does not focus on this level of detail for the electrochemical reactions that take place within a fuel cell. Instead, an empirical formulation is used to generalize a polarization curve so that the model can focus on the stack system level features rather than detailed cell level features.

2.2 Effects of Membrane Hydration

In 2001, Rowe and Li [9] investigated the transient effects of membrane hydration on a single cell's performance through mathematical modeling. This model was a one- dimensional model with the only variability passing orthogonally through the plane of the polymer electrolyte. The thermodynamic assumption of this model is that the entire cell is at the same temperature. This is the same assumption used in the model presented in this thesis and is a common assumption that has proven valid due to the relatively high conductivity of the bi-polar plates and relatively small mass and thickness of the MEA. This model concluded that water phase change affects the

dynamic temperature of a cell. Further, the model results show that the pre-humidification of the cathode air can be reduced at high loads if the anode gas humidification is high enough. This does not affect the Nexa system model since the Nexa does not humidify the anode gas at all. However, this finding may be significant for larger automotive stacks since they do typically humidify the anode gas.

2.3 Fuel Cell Stack Modeling

While the previous articles have focused on modeling single cells, Lee and Lalk [10] placed their focus on modeling full stacks. The direction that this model took was to characterize a full stack of a variable number of cells when experimental characterization had been done for a single cell. The model presents an empirical polarization curve model that is fit to known single cell parameters. This simplification of the electrochemical reaction, and heat, mass and charge transport is common in stack and system level models because it allows for focus on big picture elements rather than becoming lost in the complexity of these reactions. These empirical polarization curve formulations also allow for the stack to be scaled to any size since the calculations are typically based on current densities. To determine the waste heat of a fuel cell stack, Lee and Lalk make the assertion that any fuel energy that is not converted into electrical energy is converted into heat.

Several of the concepts implemented by Lee and Lalk's model will be utilized in the model presented in this paper. The basic concepts that will be used are the empirical polarization curve, scalable cell size and number in the stack, and Lee and Lalk's waste heat formulation.

2.4 Nexa System Modeling

In 2007, del Real, Arce, and Bordons [11] presented a model of a Nexa fuel cell system. This model includes sub-models for all of the systems on the Nexa module including a single empirical polarization curve, a simple thermal model of the stack, experimentally characterized parasitics, and an assumption that the cathode air is fully saturated when it enters the stack.

The polarization curve presented has empirical coefficients that can be calculated from experimental data. Del Real, Arce, and Bordons present the equations to calculate these coefficients in his paper. This is an improvement over other empirical polarization curves where guess and check methods are often employed to determine the coefficients.

The thermal model of the stack is very simplified. The cooling channels are modeled as a flat plane instead of as rectangular flow channels. This is a poor assumption since the convection air temperature calculations are likely to be incorrect.

The compressor and blower parasitic are modeled solely through experimental data. Transfer functions were generated from experimental data sets to very accurately model the parasitic. While this method is accurate, it is not a true mathematical model of the parasitics. No insight is gained into how the blower and compressor operate or how the system temperatures and pressures respond to changes. Additionally, this method of modeling limits this model to only the Nexa system. This model is not scalable in any way to another compressor or blower or for other pressure supply conditions. To model any other parasitic device, the user will need detailed experimental data on the new component.

The final assumption that the cathode air is fully saturated when it enters the stack is a poor assumption. While many other generic models reasonably make this assumption, the small humidity exchanger with which the Nexa system is equipped is not sufficient to raise the humidity of the cathode air enough for full saturation in dry ambient conditions. A known humidity exchanger being tested for automotive climate control applications was determined to have a mass transfer effectiveness of 35 % [13]. This is a much larger humidity exchanger and even it cannot bring slightly dry air to saturation.

The model presented in this paper is very similar to the del Real, Arce, and Bordons model. However, the model presented in this paper goes into greater detail on the compressor and blower models, the thermal model, and the humidity exchanger model.

2.5 Overview of Available Fuel Cell Models

In 2003, Haraldsson and Wipke [14] conducted an overview of available fuel cell models that were reported in papers or that were available for purchase or for free. A comprehensive list of fuel cell model features was detailed to provide guidelines for choosing the proper fuel cell modeling software for different applications. Additionally, detailed charts were presented classifying the strengths and weaknesses, the spatial dimensions, the transient abilities, and the primary phenomena studied of the models from the literature and those available commercially. Finally, Haraldsson and Wipke compared two fuel cell models side by side. One of these models was a transient, semi-empirical model developed at Virginia Tech in conjunction with the National Renewable Energy Laboratory (NREL) while the other was a steady state, theoretical model developed at Sweden's Royal Institute of Technology. Both were 0 dimensional models based on Matlab/Simulink and integrated by NREL into its ADVISOR software.

2.6 Literature Review Conclusions

Fuel cell modeling is a hot topic in the research arena. Models can range from very detailed models that focus on a small aspect of the cell as seen in the Rowe and Li model or they can focus on every aspect of a single cell as seen in the Baschuk and Li model. On the other hand, there is a great need for larger scale stack and system level models seen with the Lee and Lalk and del Real, Arce, and Bordons models. The model presented in this paper will focus on the system level aspects of a fuel cell with a specific focus on the transient thermal behavior of a system. This model will utilize the scalability of the Lee and Lalk model and a polarization curve similar to del Real, Arce, and Bordons while maintaining fully scalable system components.

3. Fuel Cell Model

This fuel cell model has five major sections. These sections include mass transport, electrical characterization, transient stack thermodynamics, water management, and parasitic losses. The focus in this model is the transient stack thermodynamics that allows for the behavior of the stack to be understood at a plethora of operating conditions. Additionally, the core of the model including the mass transport, electrical, and transient thermal sections of the model are based on a single cell building block. This allows for the scaling of the model to fit any stack configuration no matter the number of cells or effective cell area. Finally, the model is driven by gross stack current. This gives the user a better idea of the stack operating characteristics no matter what the parasitic loads happen to be. A combination of Matlab .m file code and Simulink were used to implement this model. A comprehensive block structure was used in order to easily implement code additions or to revise the code that is in place.

The time constant for the transient stack temperature is on the order of hundreds of seconds. Conversely, the transient time constants for the product and reactant flows as well as the cooling air are on the order of single seconds or fractions of a second. Therefore, these faster transient terms are ignored by this model due to their insignificance compared to the stack temperature

3.1 Mass Conservation Model

The mass conservation calculations are all based on gross current draw. This model assumes a steady flow pattern. The dynamics of increasing reactant flow streams to handle a sudden increase in current demand will be relatively fast (less than one second) compared to the slow thermal dynamics. Therefore the assumption of steady flow streams is a valid approximation. Figure 4 illustrates the reactant and product streams used in the conservation of mass equations. The figure itself depicts a cross section view of a single cell with two bi-polar plates and a membrane between.

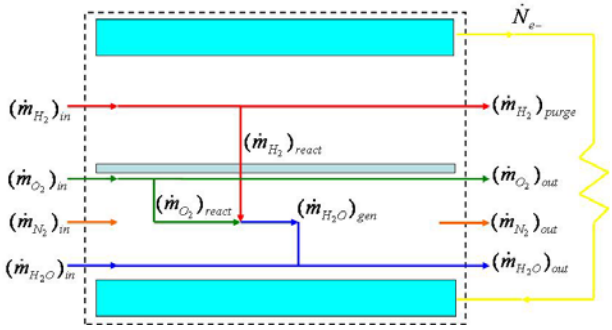

Figure 4. Conservation of mass diagram illustrating two bi-polar plates, MEA, and the product flows between them

From equations 3.1, 3.2, and 3.3, we know the chemical equations that govern the reaction of a fuel cell. All of the mass conservation equations will stem from these three simple relationships. Starting with a user defined gross current draw, electron flow is defined as

$$\dot{N}_{e-} = \frac{I_{gross}}{F}. \tag{3.1}$$

From the reaction at the anode of a single cell, we know

$$\left(\dot{m}_{H_2}\right)_{react,cell} = \frac{\dot{N}_{e-}}{2} MM_{H_2}. \tag{3.2}$$

From the reaction at the cathode and overall reaction, we know

$$\left(\dot{m}_{O_2}\right)_{react,cell} = \frac{\dot{N}_{e-}}{4} MM_{O_2}. \tag{3.3}$$

Using conservation of mass, we know that

$$\left(\dot{m}_{H_2O}\right)_{gen,cell} = \left(\dot{m}_{H_2}\right)_{react,cell} + \left(\dot{m}_{O_2}\right)_{react,cell}. \tag{3.4}$$

To determine the total flow for a stack, the single cell flow is multiplied by the number of cells in the stack. Typically, fuel cells do not consume all of the oxygen that enters them. To account for this, a stoichiometric ratio is used that is experimentally related to stack current by a curve fit such that

$$\left(\dot{m}_{O_2}\right)_{in,stack} = N_{cells} SR_{O_2} \left(\dot{m}_{O_2}\right)_{react,cell}. \tag{3.5}$$

Similarly, many fuel cell systems have hydrogen purge systems to flush contaminates and keep reactant hydrogen concentrations high. To account for this, another stoichiometric ratio is used such that

$$\left(\dot{m}_{H_2}\right)_{in,stack} = N_{cells} SR_{H_2} \left(\dot{m}_{H_2}\right)_{react,cell}. \tag{3.6}$$

The amount of air that passes through the fuel cell is important for the parasitics model specifically the compressor model. Knowing the molar oxygen/nitrogen ratio in air, we find that

$$\left(\dot{m}_{air}\right)_{in,stack} = MM_{air}\left(4.76 \frac{\left(\dot{m}_{O_2}\right)_{in,stack}}{MM_{O_2}}\right). \tag{3.7}$$

The nitrogen in the air passes straight through the system without reacting with anything. Therefore, the amount of nitrogen passing through the system is

$$\left(\dot{m}_{N_2}\right)_{sys} = MM_{N_2}\left(3.76\frac{\left(\dot{m}_{O_2}\right)_{in,stack}}{MM_{O_2}}\right) \quad (3.8)$$

Water is another key element in the mass balance in a fuel cell. The water that enters a fuel cell through the humidity in the air is found as

$$\left(\dot{m}_{H_2O}\right)_{in} = \omega_{amb}(\dot{m}_{air})_{in,stack}. \quad (3.9)$$

Conservation of mass states that the amount of water leaving the fuel cell stack must be

$$\left(\dot{m}_{H_2O}\right)_{out} = \left(\dot{m}_{H_2O}\right)_{gen,stack} + \left(\dot{m}_{H_2O}\right)_{in}. \quad (3.10)$$

From here, the electrical model will determine the polarization curve and use calculations from the mass transport model to determine the stack efficiency and heat generation.

3.2 Electrical Model

The electrical model is centered on a generic single cell polarization curve. At the system level stage of development, single cell polarization curve data should be readily available. This data is easily matched with the model's polarization curve through adjusting several parameters.

A general polarization curve is of the form

$$V_{cell} = V_{oc} - Activation\ Losses - Ohmic\ Losses - Mass\ Transport\ Losses \quad (3.11)$$

The polarization curve model is from a previous study done by Gurski [15] at Virginia Tech

$$V_{cell} = V_{oc} - b\ log\left(\frac{J}{J_{EXCHANGE}}\right) - \left(R - R_{per\,T}\left(T_{stack} - T_{ref}\right)\right) J + c\ log\left(P_{O_2}\right) + d\ (T_{stack} - Tref) \log\left(\frac{J}{J_{EXCHANGE}}\right) \text{ [15]}, \quad (3.12)$$

where $b\ log\left(\frac{J}{J_{EXCHANGE}}\right)$ is the activation loss, $\left(R - R_{per\,T}\,T_{stack}\right)J$ is the ohmic loss, and $c\ log\left(P_{O_2}\right)$ accounts for the losses due to mass transport. $d\ (T_{stack} - Tref) \log\left(\frac{J}{J_{EXCHANGE}}\right)$ represents the temperature compensation term in the model which is included to account for voltage increases and decreases due to corresponding changes in temperature. Temperature influences a fuel cells performance mainly due to the membrane's ability to become more

saturated with water at higher temperatures. V_{OC}, b, R, R_{perT}, c, d, and T_{ref} are all inputs to the model and are empirically chosen to match experimental data. T_{stack} is the stack temperature and is calculated by the model. The partial pressure of oxygen, P_{O2}, is determined experimentally and related to current draw by a curve fit. J is the current density which is determined by dividing the current draw by a user defined cell area. Since most stacks wire cells in series to boost voltage, stack voltage can be found by

$$V_{stack} = V_{cell} N_{cells}. \tag{3.13}$$

With cells wired in series, the entire stack current passes through each cell. The power output of the stack is important for stack sizing as well as understanding the stack efficiency and heat load that will be carried by the thermal systems. The cell voltage at a user defined gross stack current and active cell area is found from equation 3.12. Stack power is simply found by

$$P_{stack} = V_{stack} I_{gross}. \tag{3.14}$$

The power that is provided to the stack through the fuel is

$$P_{fuel} = \left(\dot{m}_{H_2}\right)_{in,stack} LHV_{H_2}. \tag{3.15}$$

The power provided through the fuel in reacted hydrogen is converted into two forms; electricity and heat. Therefore,

$$P_{fuel} = P_{stack} + heat. \tag{3.16}$$

The gross stack efficiency is the ratio of the output electric energy from the stack itself to the energy that went into the stack from fuel

$$\varepsilon_{stack} = \frac{P_{stack}}{P_{fuel}}. \tag{3.17}$$

The net system efficiency is discussed in the Parasitics Model section of this chapter.

These equations that make up the mass conservation and electrical models form the backbone of the transient thermal model that is the focus of the overall modeling as a whole.

3.3 Transient Thermal Stack Model

Understanding the thermal properties of a fuel cell system is critical to its development. PEM fuel cell systems are very sensitive to temperature. It is critical for a designer to be able to design the cooling system such that there is no way to overheat the stack, but also maintain the desired operating temperature. This model is a tool for ensuring that a stack has a cooling system that meets the heat rejection requirements for thermal control.

The thermal model begins with an energy balance on the stack. Figure 5 gives a visual representation of the heat streams that affect the fuel cell stack. Each mass stream is also an energy stream. Additionally, the heat generated by the electrochemical reaction and the active cooling system are taken into account in the energy balance.

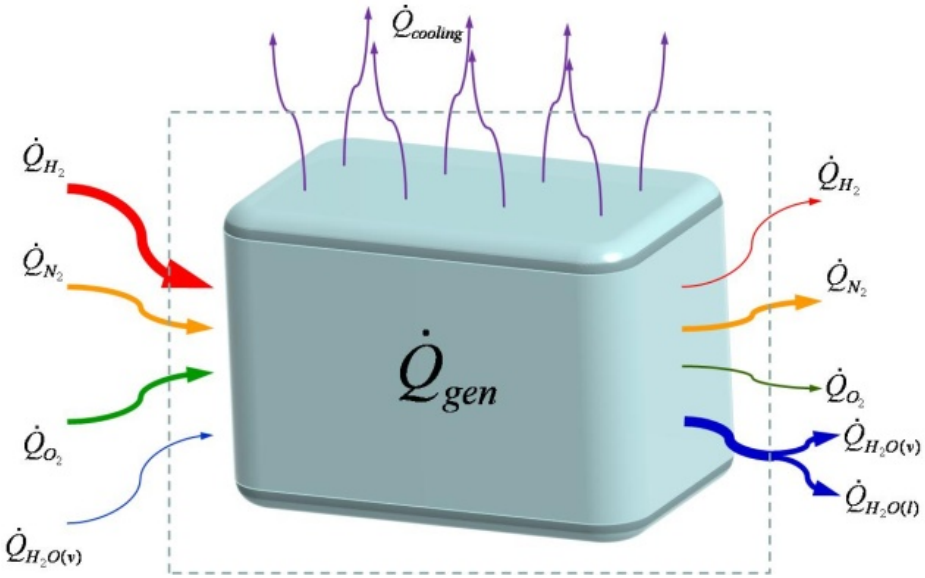

Figure 5. Heat flow diagram of a typical fuel cell system

Performing an energy balance around the entire stack yields

$$N_{cells}\left(m_{plate}c_{plate} + m_{MEA}c_{MEA}\right)\frac{\partial T_{stack}}{\partial t} = \left(\dot{m}_{H_2}\right)_{in} Cp_{H_2}\left(T_{H_2}\right)_{in} + \left(\dot{m}_{O_2}\right)_{in} Cp_{O_2} T_{amb} + \omega_{cath,in}(\dot{m}_{air})_{in} Cp_{H_2O(v)} T_{air,in} - \left(\dot{m}_{H_2}\right)_{out} Cp_{H_2} T_{stack} - \left(\dot{m}_{O_2}\right)_{out} Cp_{O_2} T_{stack} - \left(\dot{m}_{H_2O(l)}\right)_{out} c_{H_2O(l)} T_{stack} - \left(\dot{m}_{H_2O(v)}\right)_{out} Cp_{H_2O(v)} T_{stack} - \dot{Q}_{cooling} + \dot{Q}_{gen} \quad (3.18)$$

where,

$$\dot{Q}_{gen} = -\left[\left(\dot{m}_{H_2O(v)} h^0_{f,H_2O(v)} + \dot{m}_{H_2O(l)} h^0_{f,H_2O(l)}\right) - \left(\dot{m}_{H_2,react} h^0_{f,H_2} + \dot{m}_{O_2,react} h^0_{f,O_2}\right)\right] - P_{stack} \quad (3.19)$$

The enthalpy of formation terms in $\dot{Q}_{gen}$ account for the mass reacted hydrogen and oxygen and the generated water. This allows for the constant specific heat model in equation 3.18 to abide by the First Law of Thermodynamics.

The ODE 45 differential equation solver in Simulink was used to solve this differential equation.

Notice that the water leaving the stack is in both liquid and vapor states. Since these are the only two states that the water can leave the stack, we know

$$\dot{m}_{H_2O(l)} + \dot{m}_{H_2O(v)} = \left(\dot{m}_{H_2O}\right)_{out}. \tag{3.20}$$

Air can only hold a certain amount of water before it becomes saturated. Steam tables are used to find the saturation partial pressure of the water leaving the stack. A lookup table is used to implement the steam table data into the Simulink model. From this we know that

$$\dot{m}_{H_2O(v)} = MM_{H_2O}\left[\frac{P_{H_2O(v)}}{P_{cathode}}\left(\frac{(\dot{m}_{O_2})_{out}}{MM_{O_2}} + \frac{(\dot{m}_{N_2})_{sys}}{MM_{N_2}}\right)\right]. \tag{3.21}$$

The mass flow rate of liquid water out of the stack can then be found using equation 3.20. If the total amount of water leaving the system is less than the calculated maximum possible amount of water vapor leaving the system, the fuel cell exhaust stream is not saturated and all of the water leaving the stack is in the vapor state. In other words, the amount of water vapor leaving the stack equals the total amount of water leaving the stack, and the amount of liquid leaving the stack is zero. The only remaining term that needs to be calculated in the energy equation is $\dot{Q}_{cooling}$.

A typical automotive PEM system used for traction power would be liquid cooled. Due to availability, a small, 1.2 kW, Ballard Nexa air cooled stack is being used to validate this model. Therefore, the cooling system in the model is based on an air cooled system.

The modeled cooling system is based on rectangular channels running vertically through the bipolar plate. Figure 10 illustrates a top view of one of the bipolar plates. Since the channel divider material is relatively thick, its span is relatively small, and the material that most bi-polar plates are made from has high electrical and thermal conductivity, it is assumed that the channel walls are at a uniform temperature equal to the stack temperature. This leaves an array of symmetrical channels cooling channels. This symmetry, illustrated further in Figure 6, allows for the cooling effect of a single channel to be multiplied by the number of cooling channels to get the behavior of the entire array of channels.

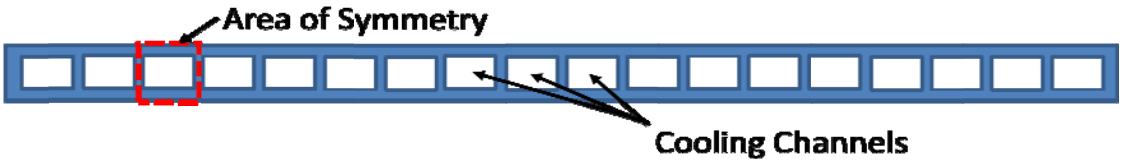

Figure 6. Top view of a bi-polar plate with symmetrical, vertical cooling channels

From the symmetry of the cooling channels and the symmetry of the cells, the total heat transfer from the cooling channels is

$$\dot{Q}_{cooling} = N_{cells} N_{channels} \dot{Q}_{channel} . \tag{3.22}$$

From this relationship, only one channel needs to be analyzed to obtain the cooling from the whole stack.

The first step is to determine if the flow through the cooling channels is laminar or turbulent. In either situation, this model assumes that there is fully developed flow through the entire length of the channel. Since the cooling channels are rectangular instead of circular, the hydraulic diameter of the channels is used

$$D_h = \frac{4A_c}{P} . \tag{3.23}$$

From this the Reynolds number is found by

$$\mathrm{Re} = \frac{\rho u_m D_h}{\mu} . \tag{3.24}$$

Except for extremely low flow speeds, the flow through the channels is turbulent. In this case, the Nusselt number is approximated as

$$Nu \approx \frac{\frac{f}{8}(\mathrm{Re}-1000)\mathrm{Pr}}{1+12.7\left(\frac{f}{8}\right)^{1/2}\left(\mathrm{Pr}^{2/3}-1\right)} \text{ [12].} \tag{3.25}$$

The friction factor, f, can be approximated for turbulent flow as

$$f \approx \left(0.790 \ln(\mathrm{Re}-1.64)^{-2}\right) \text{[12].} \tag{3.26}$$

The Nusselt number and friction factor approximations have been experimentally validated for Reynolds numbers between 3000 and 5 X 10^6 [12]. Knowing the Nusselt number, the convection heat transfer coefficient is found as

$$h = \frac{Nu\, k}{D_h}. \tag{3.27}$$

The heat transfer in the cooling channels is assumed to be steady state. This simplification was used because the thermal transients of the cooling air is much faster than the thermal transients of the stack. This assumption is justified by comparing the small thermal capacity of the small mass of air in the stack with the thermal capacity of the much larger mass of the whole stack. With this, the heat transfer in one channel is

$$\dot{Q}_{channel} = hP_{ch}L_{ch}\Delta T_{lm}, \tag{3.28}$$

where

$$\Delta T_{lm} = \frac{(T_{stack}-T_o)-(T_{stack}-T_i)}{\ln\frac{(T_{stack}-T_o)}{(T_{stack}-T_o)}}, \tag{3.29}$$

and

$$T_0 = T_{stack} - (T_{stack} - T_i)\exp(-\frac{P_{ch}L}{\rho \bar{u}_m A_{ch} c_p}h) \tag{3.30}$$

With $\dot{Q}_{cooling}$ known, all of the terms in equation 3.18 are known that are scalable with cell size and the number of cells in the stack. The only term that is unknown is the amount of water that enters the stack from the humidity exchanger.

3.4 Water Management

Water management is a critical feature of any fuel cell system. PEMFC membranes are extremely sensitive to changes in water content and the incoming reactant gas humidity. The fuel cell system used to validate this model utilizes a simple humidity exchanger to transfer water vapor from the cathode exhaust stream into the cathode reactant air stream. The model utilizes an effectiveness similar to a heat exchanger to model the humidity transfer. A diagram of the humidity exchanger is in Figure 7.

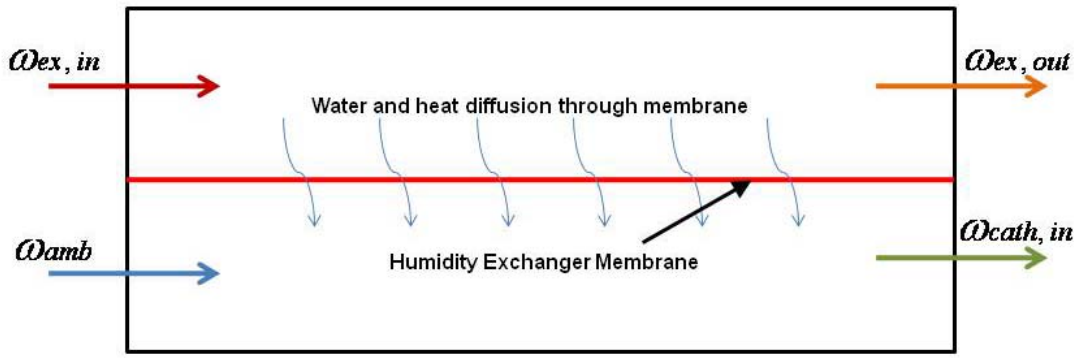

Figure 7. Humidity Exchanger Diagram

The change in water content is found by

$$\omega_{ex,in} - \omega_{ex,out} = \varepsilon_{H_2O}(\omega_{ex,in} - \omega_{amb}) = \frac{\Delta \dot{m}_{H_2O(v)}}{\dot{m}_{O_2,out} + \dot{m}_{N_2,sys}} \tag{3.31}$$

where

$$\omega_{ex,out} = \frac{\dot{m}_{H_2O(v)}}{\dot{m}_{O_2,out} + \dot{m}_{N_2,sys}}. \tag{3.32}$$

Finally, using conservation of mass in terms of water vapor, the humidity entering the stack can be found as

$$\omega_{cath,in} = \frac{\omega_{amb}\dot{m}_{air,in} + \Delta \dot{m}_{H_2O(v)}}{\dot{m}_{air,in}}. \tag{3.33}$$

Unfortunately, the validation fuel cell stack has no instrumentation to validate this part of the model. The humidity transfer effectiveness is approximated to be equal to an experimental humidity exchanger for an automotive HVAC system [13]. This is likely an aggressive approximation in that the humidity exchanger on the Ballard Nexa is significantly smaller than the HVAC humidity exchanger.

A similar set of equations is used for the heat exchange of the humidity exchanger. Following equation 3.31,

$$T_{stack} - T_{exhaust} = \varepsilon_{heat}(T_{stack} - T_{in,amb}). \tag{3.34}$$

An energy balance yields

$$(\dot{m}_{O_2,out}c_{p,O_2} + \dot{m}_{N_2,sys}c_{p,N_2} + \dot{m}_{H_2O(v)}c_{p,H_2O(v)})(T_{stack} - T_{exhaust}) = \dot{m}_{air,in}c_{p,air}(T_{air,in} - T_{in,amb}). \quad (3.35)$$

Solving for the stack inlet temperature gives

$$T_{air,in} = \frac{(\dot{m}_{O_2,out}c_{p,O_2} + \dot{m}_{N_2,sys}c_{p,N_2} + \dot{m}_{H_2O(v)}c_{p,H_2O(v)})(T_{stack} - T_{exhaust})}{\dot{m}_{air,in}c_{p,air}} + T_{amb} \quad (3.36)$$

T_{stack} is found by the differential equation 3.18. This gives all of the parameters needed to fully model the humidity exchanger. The Simulink code modeling the humidity exchanger is in Figure 14.

3.5 Parasitics Model

Parasitics are the power draws that the system requires to continue normal stack operations. The two largest power draws on the modeled stack are the air compressor supplying air to the cathode and the cooling blower. The air compressor can be modeled as a simple reversible compressor with an isentropic efficiency. The inlet and outlet pressures of the compressor are known. From this, the outlet temperature of the compressor (inlet temperature of the stack) is found by the equation

$$\frac{T_{in,s}}{T_{amb}} = \left(\frac{P_c}{P_{amb}}\right)^{(k-1)/k}. \quad (3.37)$$

The actual compressor outlet temperature will be greater due to the inefficiencies of the compressor characterized by the isentropic efficiency. For an ideal gas assuming constant specific heat, the isentropic efficiency is defined as

$$\eta_{comp} \cong \frac{T_{in,s} - T_{amb}}{T_{in,a} - T_{amb}}. \quad (3.38)$$

From this, the actual output temperature is

$$T_{in,a} = \frac{1}{\eta_{comp}}\left(T_{in,s} - T_{amb}\right) + T_{amb}. \quad (3.39)$$

Knowing the actual compressor outlet temperature, the compressor power is found by

$$P_c = \varepsilon_{el,comp}\dot{m}_{air,in}(Cp_{air}\left(T_{in,a} - T_{amb}\right) + \frac{1}{2}u_{comp}{}^2), \quad (3.40)$$

where

$$u_{comp} = \frac{\dot{m}_{air}}{\frac{1}{4}\pi {D_{comp}}^2 \rho_{(P,T)_{comp}}} \tag{3.41}$$

The equations that govern the blower model are very similar to the compressor equations. The velocity that the air flows through the humidity exchanger is known. Therefore, the pressure drop across one of the cooling channels can be found as

$$\Delta P_{bl} = f \frac{L_{ch}}{D_h} \frac{{u_{bl}}^2}{2g} \tag{3.42}$$

Knowing this, the outlet temperature of the blower is found as

$$\frac{T_{bl}}{T_{amb}} = \left(\frac{\Delta P_{bl} + P_{amb}}{P_{amb}}\right)^{(k-1)/k} \tag{3.43}$$

The blower is assumed to be isentropic and the efficiency term encompasses both the isentropic efficiency and the electrical efficiency giving the equation

$$P_{bl} = \varepsilon_{bl} \dot{m}_{air,in} (Cp_{air}(T_{bl} - T_{amb}) + \frac{1}{2}{u_{bl}}^2). \tag{3.44}$$

This approach was taken due to the inability to accurately measure the outlet temperature of the blower. The heat from the stack will heat up the blower ducting leaving no way to determine if the temperature rise is due to the compressor or from heating due to the stack.

4. Validation Hardware and Instrumentation

The hardware used to validate this model consists of a Nexa fuel cell system, electrical load, and measurement hardware. A schematic of the test setup is in Figure 8, while an actual picture is in Figure 9.

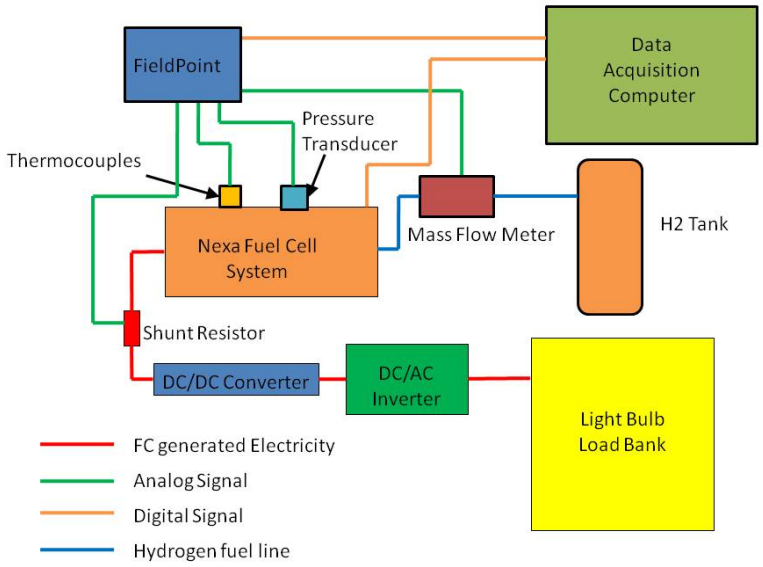

Figure 8. Schematic of the test setup

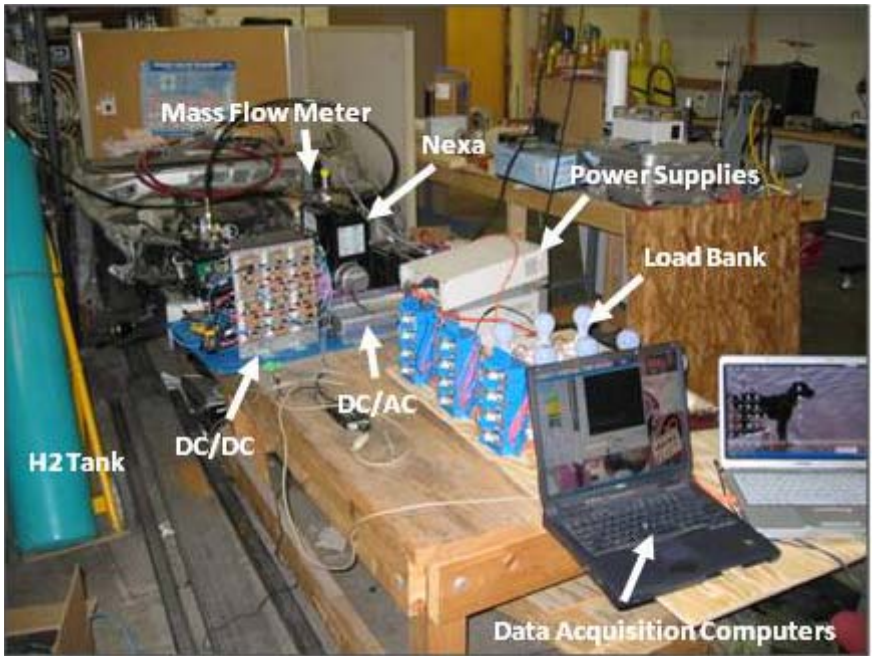

Figure 9. Picture of the test setup

4.1 Fuel Cell

Availability dictated that the fuel cell used for validation be a Ballard Nexa fuel cell system. The specifications of the system are found in Table 1. Bipolar plate parameters are in Table 2. The Nexa is a complete fuel cell system with its own controller. The only thing the system needs to run is a supply of hydrogen and a 24 V power supply for start-up and shut-down operation. The fuel cell is visible in Figure 15.

Table 1. Ballard Nexa specifications

Rated Net Power	1.2 kW
Cooling	Air cooled
Blower Type	Centrifugal
Compressor Type	Twin Screw
Fuel	H_2 gas (99.99% pure)
Fuel Supply Pressure Range	70 – 1720 kPa
Ambient Air Temperature Range	3 - 40 °C
Voltage Output	22 – 50 V

Table 2. Nexa Bi-polar plate parameters

Mass	86 g
Specific Heat	879 J/kg-K
Anode:	
channel length	226.4 cm x 2 channels
channel width	1.143 mm
channel depth	0.4318 mm
flow x-section area	0.494 mm^2
Flow channel GDL contact area	51.76 cm^2
GDL plate contact area	69.8 cm^2
Cathode:	
Channel 1 length	88 cm x 2 channels
Channel 2 length	87.6 cm x 2 channels
Channel 3 length	88.6 cm x 2 channels
Total channel length	528.4 cm
channel width	1.143 mm
channel depth	0.6858 mm
flow x-section area	0.784 mm^2
Flow channel GDL contact area	60.40 cm^2
GDL plate contact area	61.1 cm^2
Cooling Channels:	
Legnth	12.56 cm
Width	4.19 mm
Depth	3.10 mm

4.2 Electrical Load

An electrical load is needed to test the full power range of the fuel cells. This electrical load must have a wide range of power settings, be able to adjust power loads "on the fly", and most importantly be inexpensive. The load setup that was decided on was a bank of 12, 100 W light bulbs. To make the output power of the fuel cells fully compatible with the fuel cells, power conversion devices were needed. To accomplish this, a bank of DC/DC converters and a DC/AC inverter were used.

4.2.1 DC/DC Converters. Vicor donated two full banks of DC/DC converters to be used with the Nexa system for an in car auxiliary power system that the Hybrid Electric Vehicle Team uses as a demonstration exhibit. These DC/DC converters condition the unregulated DC voltage from the fuel cell to regulated 13.8 V DC that can be used in any 12V electrical circuit. The converter bank consists of 12, 100 W converter modules. There is one master module that controls the output of 11 slave modules. For heat dissipation, the modules are mounted to a ¼ inch sheet of aluminum. The specifications of the Vicor converters are in Table 3.

Table 3. Vicor DC/DC converter specifications

Model	VI-222-EW
Number of Modules	12
Rated Power each	100 W
Input Voltage	36 V nominal (21-56 V)
Output Voltage	15 V trimmed to 13.8 V
Operating Temperature	-10 °C – 85 °C
Efficiency	78 – 88 %

4.2.2 DC/AC Inverter. To generate the 120 VAC, 60 Hz household power required by the array of light bulbs used as the load, a large DC/AC inverter is needed. Due to the automotive and marine market, inverters with 12 VDC inputs are very common and fairly inexpensive. An AIMS inverter was chosen for its 1250 W continuous power rating and price. The specifications for this inverter are in Table 4.

Table 4. AIMS DC/AC inverter specifications

Model	PWRINV1250W
Continuous Power Rating	1250 W
Surge Power Rating	3100 W
Input Voltage	10 – 15 V
Output Voltage	120 VAC/60 Hz
Output Wave Form	Modified Sine
Operating Temperatures	-15 °C – 55 °C
Efficiency	> 90 %

4.2.3 Load Bank. Common household light bulbs were chosen for a load bank for cost reasons as well as being able to have numerous power points that can be adjusted "on the fly." A bank of 12, 100 W light bulbs with household switches on each bulb make up the load bed. This allows for the full power range of the fuel cell to be used at approximately 100 W steps. As will be shown in the validation of Chapter 5, the step size is higher than 100 W due to the losses in the power conditioning devices.

4.3 Data Collection

Two separate devices were used to collect data from the fuel cell. The Nexa system has built in data collection. To supplement this, additional transducers were added to the fuel cell. These transducers were collected using National Instruments Compact FieldPoint modules.

4.3.1 Built In Data Collection. The Nexa system has built in data collection. The Nexa sends this data through an RS 434 formatted port. The data is then converted to an RS 232 format through a converter to be read into a serial port on a computer. Ballard provides NexaMon software to read and log this data. A screenshot of the NexaMon software is in Figure 10. A list of the parameters that is recorded by the NexaMon software is in Table 5. There are only a few additional parameters that are needed to fully validate the model. For these parameters, additional instrumentation and collection hardware was needed.

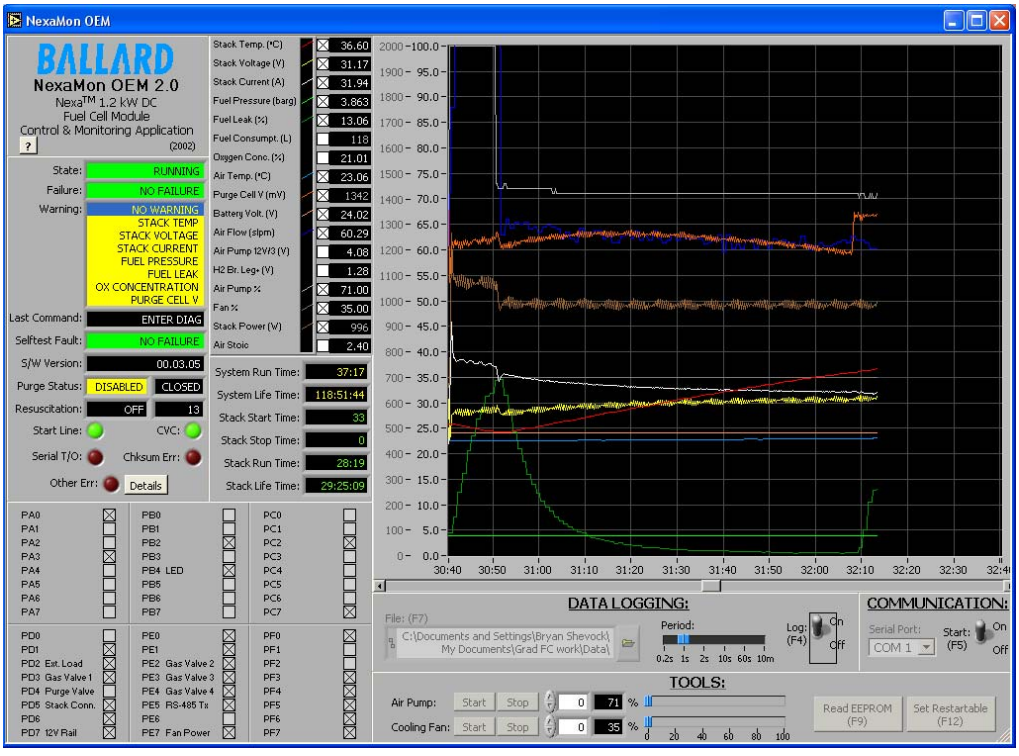

Figure 10. Screenshot of the NexaMon user interface

Table 5. NexaMon data collection parameters

Parameter	Units
Stack Temperature	°C
Stack Voltage	V
Stack Current	A
Fuel Supply Pressure	barg
Fuel leak	% of LFL
Total Fuel Consumption	Standard L
Oxygen Concentration	% of air
Ambient Air Temperature	°C
Purge Cell Voltage	mV
Start-up/Shut-down battery voltage	V
Cathode Air Flow	slpm
Air Pump (12V/3)	V
H2 Br Leg+	V
Air Pump Power	% of max
Blower Power	% of max
Stack Power	W
Air Stoichiometric ratio	

4.3.2 National Instruments Compact FieldPoint. Additional transducers were required to fully validate the model. To collect this data, a National Instruments Compact FieldPoint module was used. This blue module is clearly visible in Figure 8. An Ethernet interface was used to connect the Compact FieldPoint with a computer. From here, LabVIEW was used to collect, scale, and record the data. Two analog input modules and a thermocouple module was needed to input all of the required data into the FieldPoint Real Time module. A list of the parameters that each FieldPoint module read is in Table 6. The front panel of the LabVIEW .vi is in Figure 11.

Table 6. FieldPoint modules and parameters read

Field Point Module	Channel	Parameter
TC-120@1	0	Compressor Inlet Temp
TC-120@1	1	Compressor Outlet Temp
TC-120@1	2	Exhaust Outlet Temp
TC-120@1	3	Cooling Air Outlet Temp
TC-120@1	5	Net Current
AI-100@2	0	Compressor Pressure
AI-100@2	2	H2 Mass Flow Rate
AI-100@3	0	+1/2 Stack Voltage
AI-100@3	1	-1/2 Stack Voltage

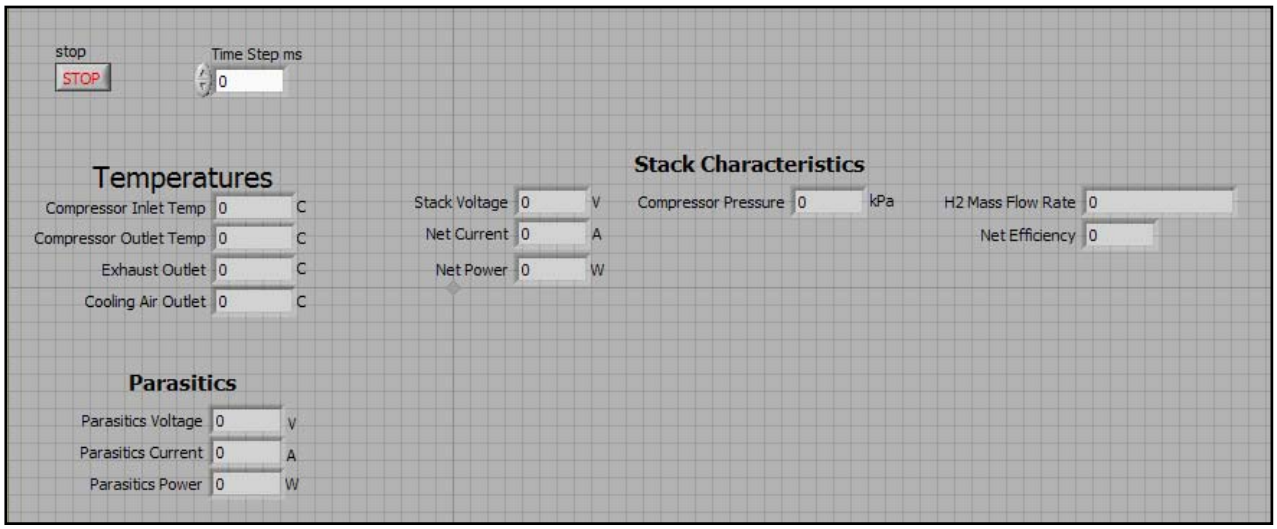

Figure 11. LabVIEW .vi front panel

4.4 Fuel Cell Instrumentation

Additional transducers are required to fully validate the stack model. These transducers include a hydrogen mass flow meter, pressure transducer on the output of the compressor, and several thermocouples to complement the temperatures recorded by the NexaMon software.

4.4.1 Hydrogen Mass Flow Meter. A hydrogen mass flow meter was added to the fuel supply line to validate part of the mass transfer model as well as defining the hydrogen stoichiometric ratio. A Sierra instruments model that reads up to 40 slpm of hydrogen flow was used due to availability. Specifications for the mass flow meter are in Table 7. The meter outputs a voltage of 0 to 5 volts increasing linearly with flow. LabVIEW code was used to convert this raw output into kg/s for data collection and analysis.

Table 7. Specifications for the Sierra Instruments mass flow meter

Gas	H2
Flow Rates	0 – 40 slpm
Calibrated inlet pressure	400 kPa
Accuracy	± 0.04 slpm (1% of full scale)

4.4.2 Compressor Pressure Transducer. To understand and characterize the cathode air compressor parasitics, a pressure transducer was added to the outlet of the compressor. This transducer allows for an understanding of how the stack controller increases pressure with respect to the current draw on the stack. The greater the cathode air pressure, the greater the performance of the stack due to an increase in oxygen concentration at the reaction sites.

Therefore, it is expected that at larger current loads, the compressor will operate at higher pressures. An Omega pressure transducer was chosen due to availability and its operating range of 0 to 15 psi gauge. The specifications for the pressure transducer are given in Table 8. The compressor transducer uses a current output that varies linearly with pressure. This current output was read into the Compact FieldPoint module and calibrated using LabVIEW software.

Table 8. Specifications for the compressor pressure transducer

Range	0 – 15 psig (103.4 kPa)
Excitation Voltage	12 – 25 V
Output	4 – 20 mA
Temperature Range	-55 °C – 105 °C
Accuracy	0.045 psi (0.310 kPa)

4.4.3 System Temperature Thermocouples. To fully validate the thermal model of the full system, additional temperature measurements were needed in addition to the stack and ambient temperatures that are collected by the Nexa controller and sent to the NexaMon software. The compressor model validation required thermocouples placed at both the inlet and the outlet of the compressor. The humidity exchanger validation required a thermocouple on the exhaust outlet of the stack. Finally, the thermal model required a thermocouple at the cooling air outlet of the stack. Type J Omega thermocouples were chosen for easy monitoring by the Compact FieldPoint system and their effective temperature range. Specifications for the thermocouples chosen are in Table 9. The thermocouples were installed into a Compact FieldPoint thermocouple module for data collection. Calibration was done using LabVIEW software.

Table 9. Thermocouple specifications

Thermocouple Type	J
Operating Temperature Range	0 °C – 750 °C
Error	± 2 °C

4.4.4 Net Current and Output Voltage. To better understand the parasitic losses of the stack, the net current of the system was monitored with a shunt resistor. The resistor was rated at 0.001 Ω giving a voltage across the resistor of one mV for every amp of current. This voltage was read into a thermocouple module on the Compact FieldPoint block to insure accurate readings for such small voltages. Calibration and scaling was done using LabVIEW software.

Stack output voltage was monitored to ensure the accuracy of the reported stack voltage in the NexaMon software. Unfortunately, a Compact FieldPoint analog input module that could handle up to 45 VDC was not available for this project. Instead a circuit of four, 100 kΩ resistors was used to monitor the stack voltage in two stages. A schematic of the circuit used is found in

Figure 12. This circuit allowed for two voltage measurements, which were approximately half of the stack voltage, to be taken and added together to obtain the full stack voltage. Due to the common ground configuration of the Compact FieldPoint analog input module, the voltage measurement had to be taken with the ground in the middle of the resistor array to be compatible with other measurements that this module was collecting. The result was that one of the stack voltage measurements was positive and one was negative. This was corrected using LabVIEW software. While this technique doubles the amount of error in the measurement, its purpose is only to ensure that the output of the stack is the true stack voltage and that there is not a significant voltage drop in the system before the output wires. Once the NexaMon reported voltage was verified, it was the value used in all calculations.

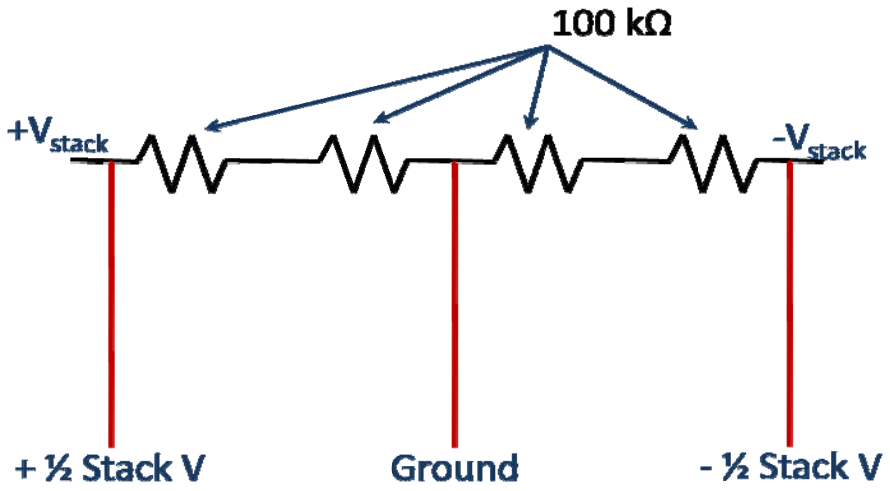

Figure 12. Schematic of the circuit used for the stack voltage measurement

4.4.5 Anemometer. The thermal model required exhaust air speed calculations for full validation. A La Crosse anemometer was chosen for cost and measurement unit flexibility. The specifications for this anemometer are in Table 10.

Table 10. La Crosse anemometer specifications

Model	EA - 3010
Air speed measurement range	0.44 – 67 mph (0.2 – 30 m/s)
Resolution	0.1 for all units
Operating Temperature Range	-29.9 °C – 59 °C

5. Model Validation Procedures

The first step in validating the fuel cell model was to calibrate and determine the repeatability of each added sensor. Data collected from the NexaMon software was assumed to be valid due to the inaccessibility of the transducers. From there, each section of the model was compared to real world data to determine the accuracy and robustness of the model.

5.1 Transducer Calibration

All transducers were assumed to be linear in their outputs and each transducer has specifications insuring that this is a reasonable assumption.

5.1.1 Hydrogen Mass Flow Meter. The calibration of the mass flow meter was done for hydrogen at a supply pressure of 400 kPa at the factory. This calibration was assumed to be valid because there is no other way to accurately measure mass flow. The meter was verified to have zero offset in the factory calibration.

5.1.2 Compressor Pressure Transducer. The pressure transducer was calibrated against a dial pressure gauge. The calibration curve is in Figure 13.

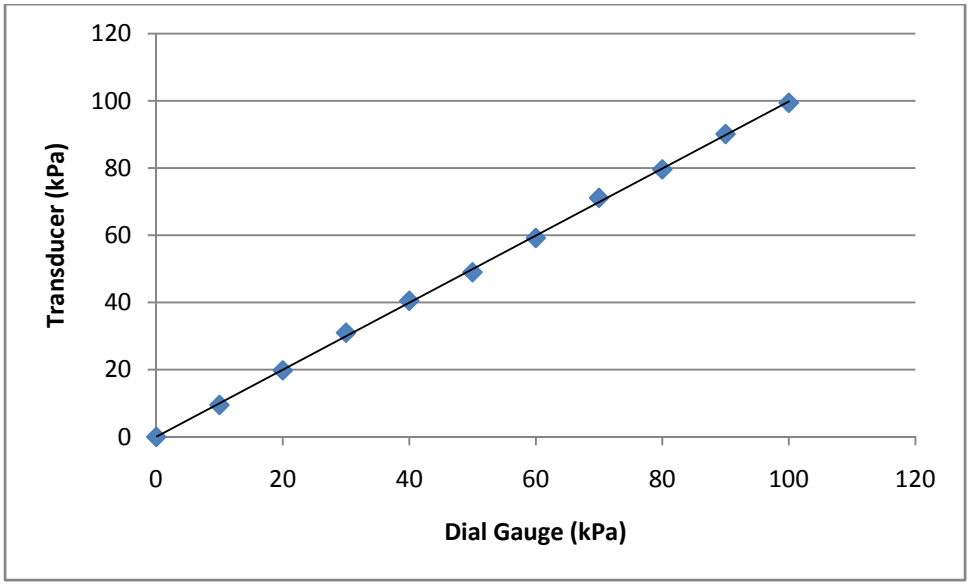

Figure 13. Compressor pressure transducer calibration curve

5.1.3 Thermocouple Calibration. The thermocouple output was compared against the temperature reading on the anemometer. Thankfully, the temperature in the lab where the test setup was located differed greatly from the outside temperature. This temperature fluctuation was used to calibrate the thermocouples. The whole stack was allowed to reach steady state

temperatures indoors and outdoors. The indoor soak was overnight and the readings were taken early in the morning before the room had time to heat up from the sun. For the outdoor temperatures, the compressor was run slowly to cycle cold air into the stack since the test bench could not be left outside overnight. It was found that each thermocouple had a similar offset and minimal slope variation. All variation was within the 2.2 °C error of the thermocouples. The offset likely came from the Compact FieldPoint since the shunt voltage measurement also had an offset. The thermocouple offset of 1.6 °C was removed electronically. While this method for calibration is not as precise as possible, no temperature chamber was available to conduct a proper calibration. While not perfect, this method seemed to verify that there was no slope variation. This is the expected result from a properly functioning thermocouple. The ambient temperature calibration data from five days with different ambient temperatures is found in Figure 14.

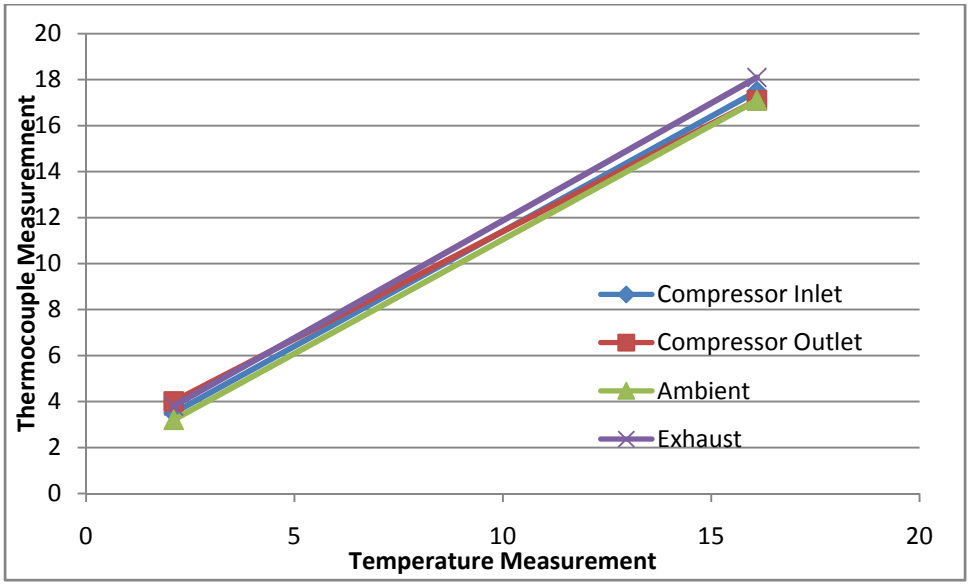

Figure 14. Thermocouple calibration data

5.1.4 Current Measurement. The net current measurement from a shunt resistor was calibrated using a digital multimeter to measure millivolts across the shunt. Like the thermocouple measurement, there was a slight offset in the data of 1 mV. The voltage calibration curve of the measurement is found in Figure 15. To ensure the resistance of the shunt was actually 0.001 Ω, an additional calibration was preformed. This calibration is found in Figure 16. This curve only goes to 10 A due to the limits of the multimeter. The results show that for each millivolt across the shunt there is to 1A passing through the shunt giving a resistance of 0.001 Ω.

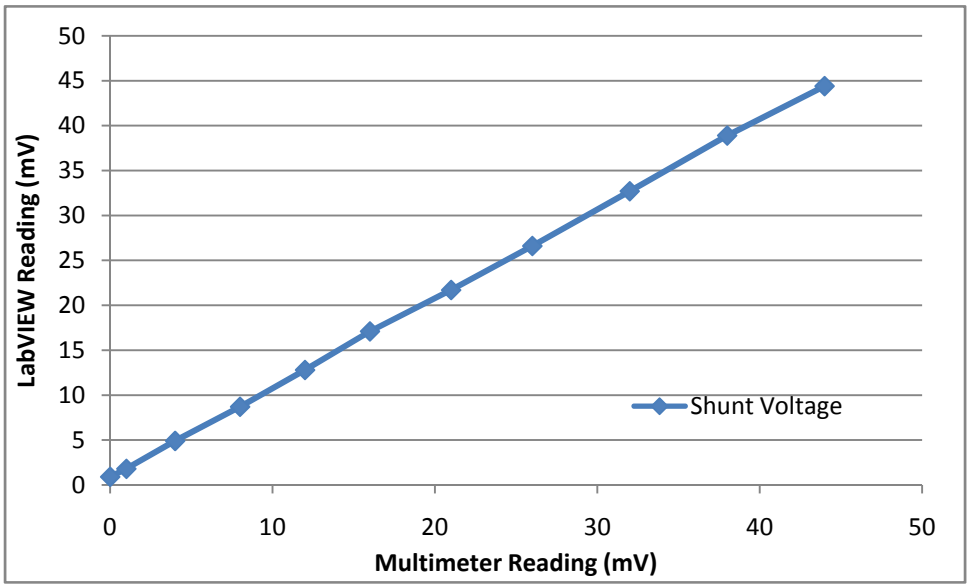

Figure 15. Shunt voltage calibration data

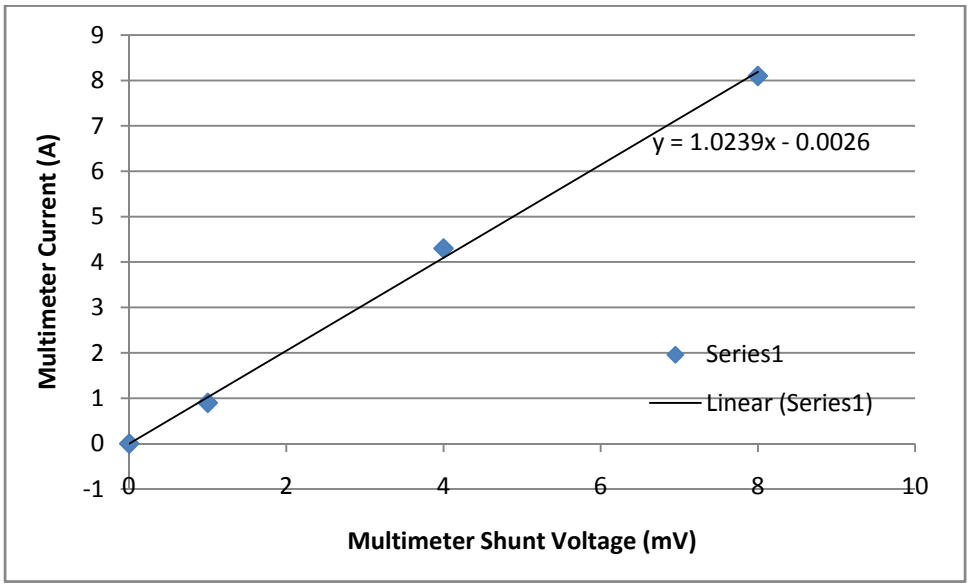

Figure 16. Shunt resistance validation

5.2 Mass Conservation Model Validation

There are three distinct areas of the mass conservation model that require validation. These include the anode hydrogen flows, cathode air flow, and product water generation. The water vapor exhaust is difficult to measure, so the liquid water generation was used to validate this part of the model.

The first step in validating the mass conservation model was to compare the results to a steady state excel spreadsheet model created previously. The steady state excel spreadsheet contained all of the mass conservation equations and electrical equations detailed in sections 3.1 and 3.2 This comparison better ensured that no calculation or programming errors were present in the model. The Simulink and steady state excel model's agree exactly reducing the chance that a typographical error was made.

The mass flow meter was used to validate the hydrogen flow section of the mass conservation model. A good metric for validation is the stoichiometric ratio of the anode hydrogen. This parameter is expected to be slightly above 1. A stoichiometric ratio of one indicates that all of the hydrogen that enters the stack is converted to electricity. Since there are likely small losses of hydrogen due to imperfect seals and potential permeation through the membrane, the hydrogen stoichiometric ratio is expected to be slightly above one. A plot of hydrogen stoichiometric ratio is given in Figure 17. Another important note is that the Nexa system purges the anode gas periodically to remove contaminants from the hydrogen channels at the anode. The purged hydrogen is exhausted through the cooling air channels to be sufficiently diluted for safety. This purging is ignored by the model since the purged amount of hydrogen is sufficiently small as to not affect the thermal model. A graphical example of this hydrogen purge is seen in Figure 18. The spikes in hydrogen mass flow rate that show the hydrogen purge process are clearly visible while the current remains steady.

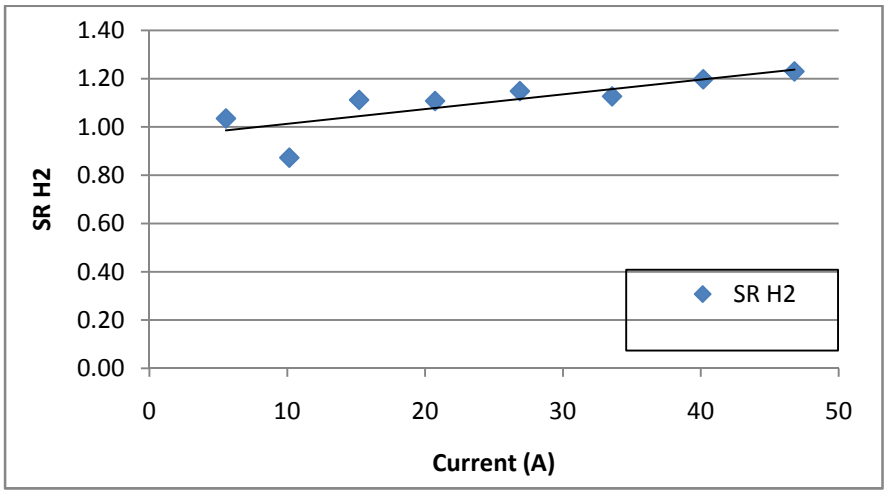

Figure 17. Hydrogen stoichiometric ratio versus gross current draw

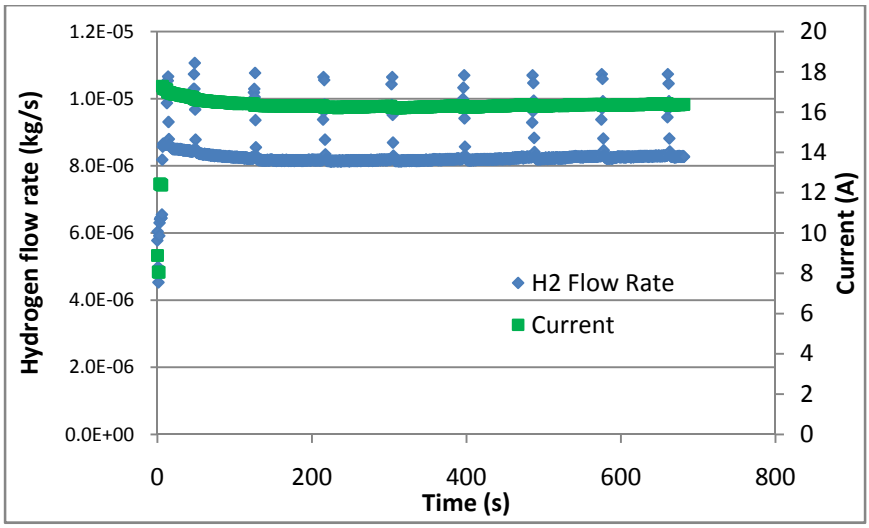

Figure 18. An example of hydrogen purge

The NexaMon reported cathode air flow rates were used to validate the cathode air portion of the mass transport model. The calculations that the model uses to determine actual flow rates is similar to the hydrogen conservation of mass model in that a stoichiometric ratio is used to determine the amount of excess air the system flows through the stack. Unlike the anode hydrogen, the system flows a much larger amount of excess air through the system. This excess air helps to maintain a higher partial pressure of oxygen at the cathode reaction sites which is critical to the performance of the stack. Also, the extra volume of air helps to clear out the flow channels of the product water that builds up in the stack. For validation purposes, the stoichiometric ratio of oxygen at the cathode is used just as the stoichiometric ratio of hydrogen was used to validate the anode hydrogen calculations. Expected stoichiometric ratios of oxygen should always be greater than 2. Very large ratios are expected at idle and low loads due to the compressor's inability to operate below a certain speed and flow rate. To determine the stoichiometric ratios from experimental data, the measured flow rate of oxygen is divided by the calculated consumed oxygen. If the resulting stoichiometric ratios agree with the expected results, the model is deemed valid to the greatest degree possible with the available diagnostic equipment. A plot of the stoichiometric ratios of oxygen versus stack current load is in Figure 19. As expected, the idle ratio is very large, presumably due to the compressors inability to operate at very low flow rates. From here, the stoichiometric ratios tail off to a value of around 2.4. This is above but close to the expected value of 2. The compressor pressure increases more steeply with current draw yet maintains a constant stoichiometric ratio. This steeper pressure rise is to maintain enough oxygen in the stack to meet current demand. Based on the instrumentation available, the cathode air portion of the mass transport model is deemed validated.

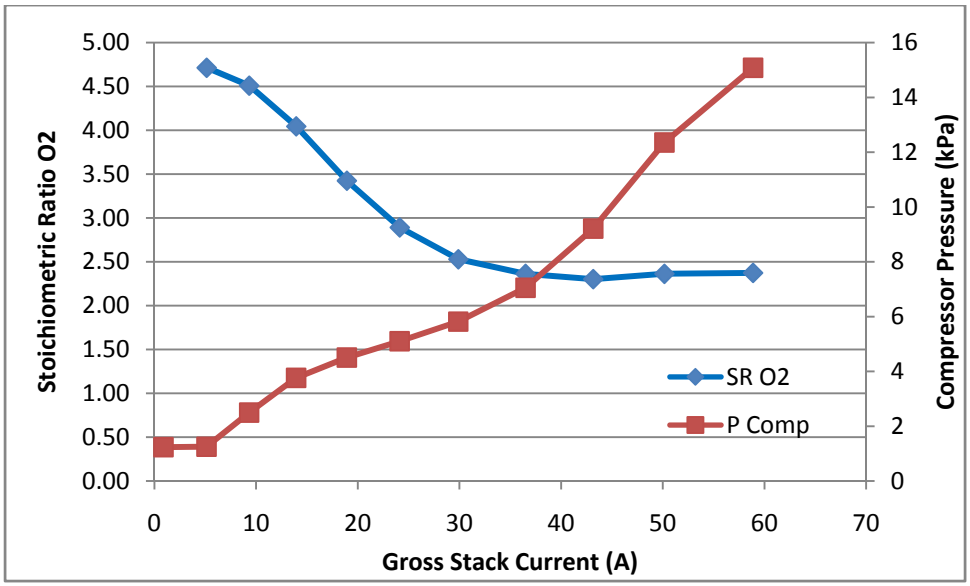

Figure 19. Oxygen stoichiometric ratio and compressor pressure vs flow rate.

The final portion of the mass conservation model that requires validation is the product water generation portion. This is by far the most difficult portion of the mass conservation model to validate due to the inability to measure all of the required parameters. The Nexa fuel cell system gives off a significant amount of liquid water as exhaust. For validation, the product water was collected for a period two minutes and compared to the calculated amount of water that should be generated. Unfortunately, there is no way to measure the water vapor in the exhaust with the instrumentation available. Additionally, there is no way to determine how much water is stored in the humidity exchanger. These factors increase the amount of error in this validation technique. This is not a problem since the hydrogen and oxygen mass conservation models have already been determined to be valid, and these models are directly related to the water production model by conservation of mass given by equation 3.4. For this validation step, the stack was run at constant load for 5 minutes and the resultant liquid water was weighed. From this, the average water generation was calculated and compared to the model. The model assumes a steady state water production and no water storage in the stack or humidity exchanger. The results of this validation procedure for several constant current loads are in Figure 20. Despite the high potential for error in this validation procedure, the experimental results follow the same trend as the modeled results. The modeled results are always higher than the experimental results. This is expected since the experimental results do not take into account the generated water given off as vapor. Additionally, the difference between the modeled data and experimental data increases with current. This is expected since the higher stack temperatures at the higher loads increases the potential for water to exit the stack as vapor. The product water generation validation produced results that matched the trend of the experimental data. Therefore, the water production portion of the mass transport model is deemed validated.

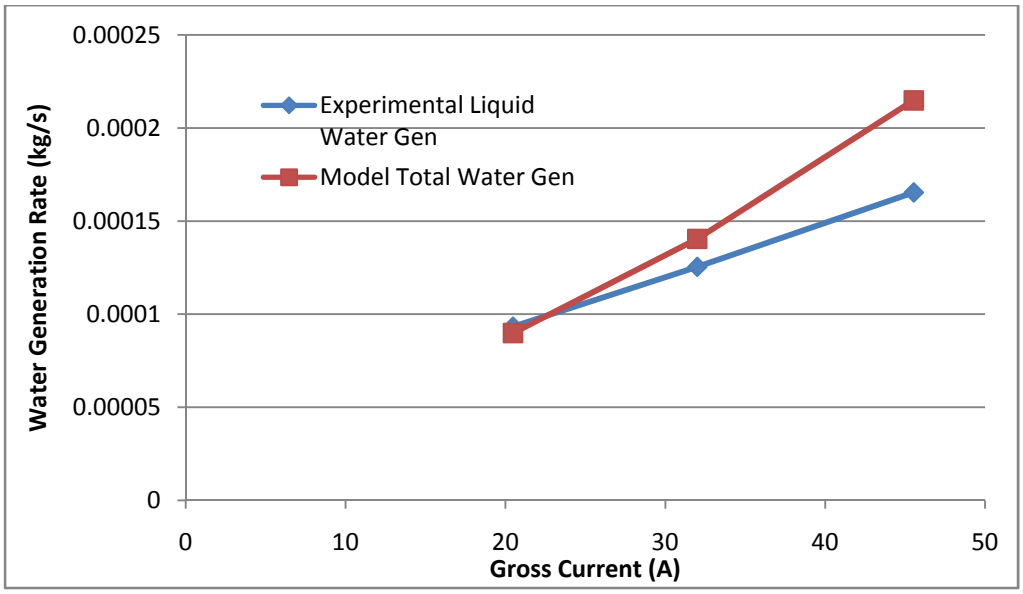

Figure 20. Water generation for several current levels.

5.3 Polarization Curve Validation

The polarization curve was determined empirically by equation 3.12. This empirical equation was compared to experimental data to determine the empirical coefficients. A list of the chosen coefficient values is found in Table 11. A plot of the polarization curve is in Figure 21. The green "Documented" data points were obtained from the Nexa documentation. The change in temperature explains the wide range of experimental voltage. The curve fit shown is fit to the coolest temperature and therefore lowest voltage at each load point. Once the polarization curve coefficients were determined for these points, the stack was heated to 56°C by operating the stack at high load to determine the temperature effect coefficients of the polarization curve.

Table 11. Polarization curve coefficients

B	0.115
R	0.4
RperT	0.009
Pcoef	0.3
Tcoef	0.00002

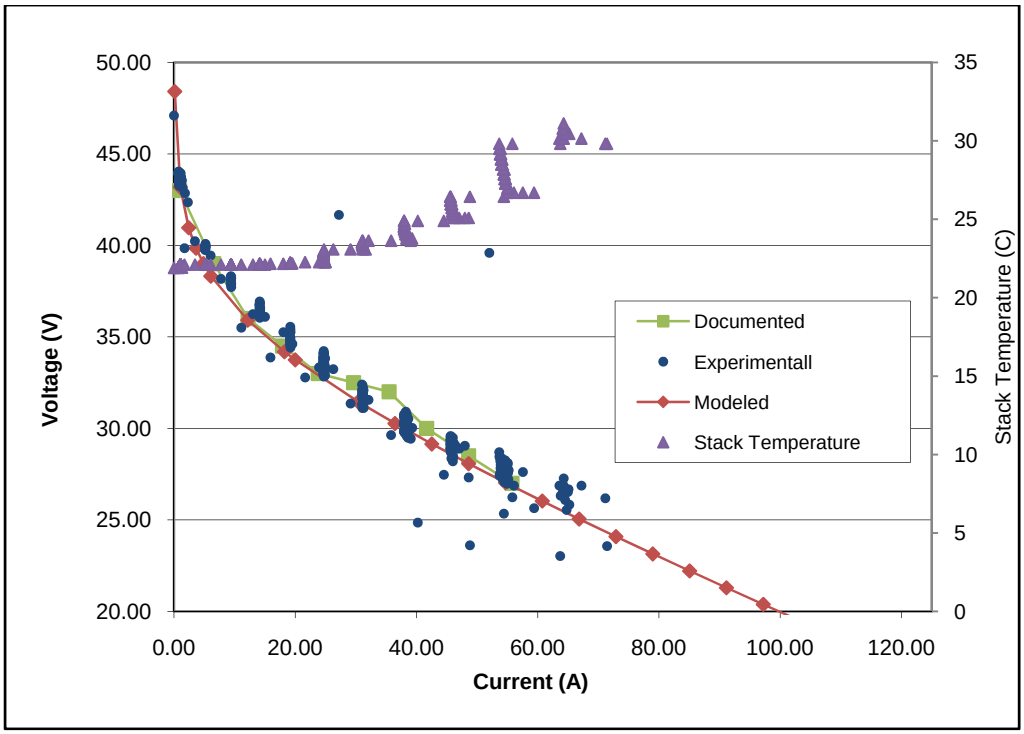

Figure 21. Polarization curve

5.4 Transient Thermal Model Validation

There were several parameters that needed to be validated to determine the validity of the transient thermal model. The primary parameters for this validation are stack temperature and cooling air outlet temperature. These are the only two independent temperatures utilized by the model. The first step to validating the thermal model is to analyze the steady state model temperatures with experimental data. A table comparing these values is in Table 12. The steady state model values agree closely with the experimental data.

Table 12. Steady state validation

Gross Current	Cooling Speed (m/s)	Stack Temp C	T predicted C	Error in T C
5.47	2.2	22.69	21.3	-1.39
10.1	2.2	28.32	26.3	-2.02
15.6	2.2	34.12	32	-2.12
20.59	2.2	39.72	38.4	-1.32
26.17	2.3	44.56	44.5	-0.06
32.75	2.4	51.19	51.8	0.61
40.27	2.6	56.19	59.8	3.61

It is also important that these parameters be validated on heating and cooling cycles to fully validate them. To accomplish this, the stack was introduced to a step current load and allowed to heat up due to the current load until the stack reached a near steady state condition. Then, the load was removed from the stack, and the stack was allowed to cool to a near steady state condition. The corresponding simulation was run and the results were compared with the experiment. This was repeated for several different step current levels. The stack temperature results are shown in Figure 22 while the cooling air temperature results are shown in Figure 23. The modeled stack temperature agrees relatively closely with the experimental results. The largest error is only 3 °C. The correlation for the cooling air outlet temperature is not quite as good but still provides a reasonable approximation. The largest difference in the modeled cooling air temperature and the experimental results is 7 °C, and the trend in the modeled results matches those of the experimental results. This may be due to the assumption in the model that the entire perimeter of the cooling channel is at the stack temperature. From these results the transient thermal model can be deemed validated.

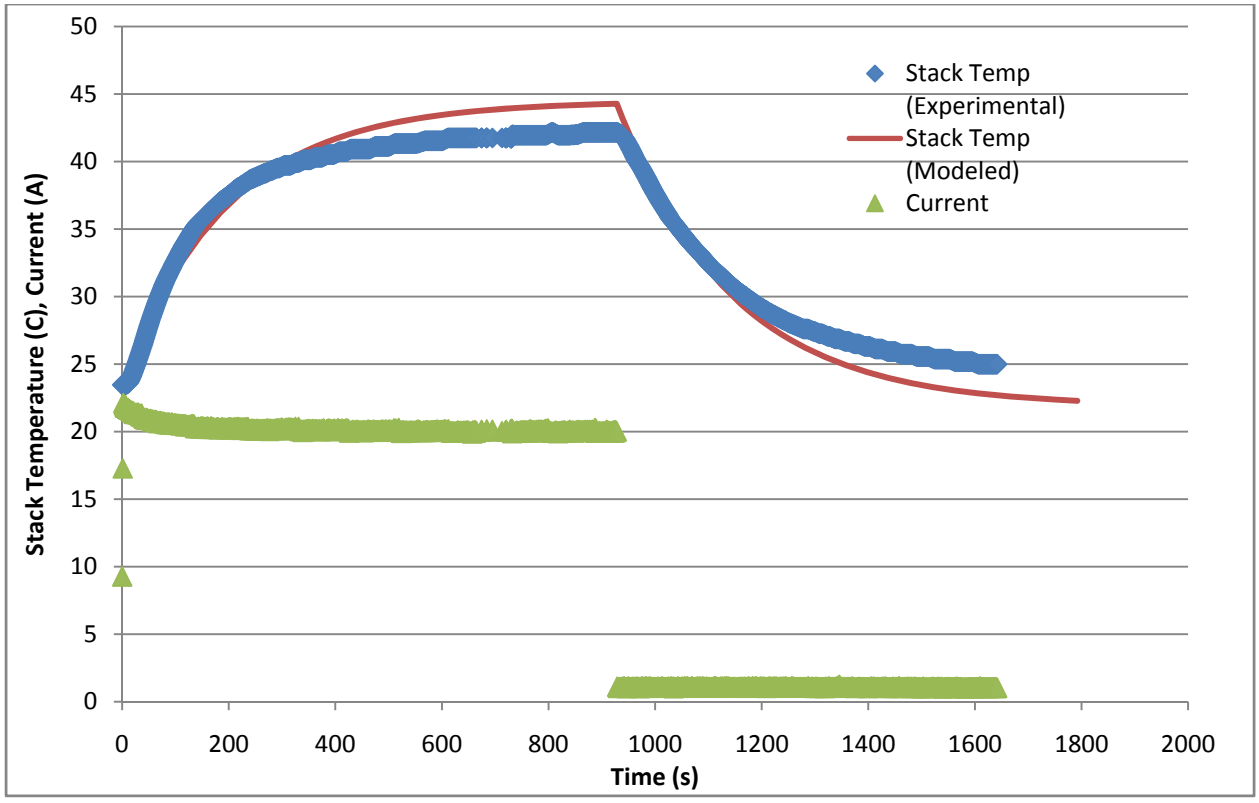

Figure 22. Stack temperature validation results

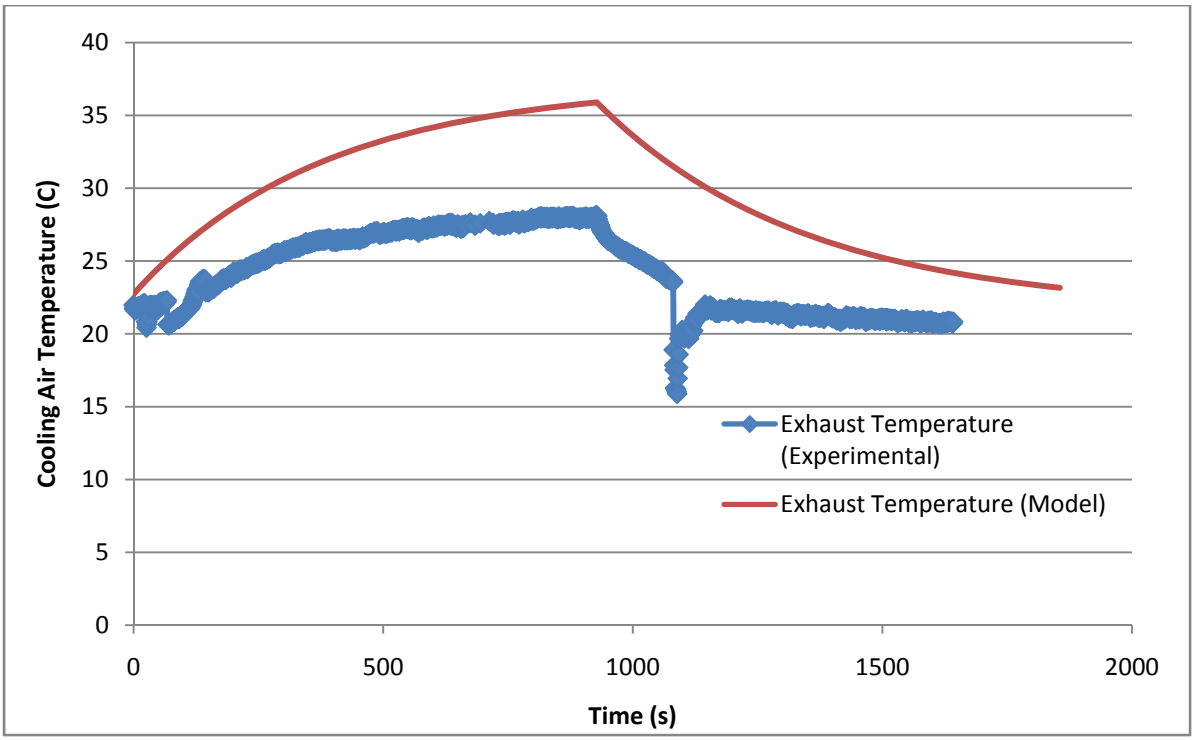

Figure 23. Cooling air temperature validation results

5.5 Water Management Model Validation

The water management model is the most difficult model to validate due to the available instrumentation. Due to the level of integration of the humidity exchanger, there is no way to get instrumentation into the air flow stream entering the stack. Because of this, the humidity of the air entering the stack is experimentally unknown. To compensate for this, del Real, Arce, and Bordons [11] assumed that the air entering the stack was saturated. For the small size of the humidity exchanger and the low temperature operation of the stack, this is most likely a poor assumption. For this thesis work, the water transfer effectiveness for the humidity exchanger is assumed to be similar to a Daius Analytic Corporation humidity exchanger in development for automotive climate control applications. The US Department of Energy did a study on this heat exchanger for efficiency gains in the climate control system of an automobile in 2005 [13]. Based on these measured values, an effectiveness of 0.3 was used for this model. This assumption is based on testing, and, therefore, is more accurate than del Real, Arce, and Bordons' assumption. The impact of this new assumption on the overall performance of the model is very small considering that an empirical fit is being utilized for the polarization curve of the model, and the energy contained in the water vapor entering the stack is small.

5.6 Parasitics Model Validation

The final section of this model that needs validation is the parasitic model. The compressor parasitics and the blower parasitic model need to be validated. The first step to this model validation was collecting data from the blower and compressor separately. This was accomplished by running the compressor and blower at several points along their range of operation separately and without the stack generating current. NexaMon allowed for this operation of the parasitic systems. From here, the efficiencies of the two parasitic systems were adjusted in the model to somewhat match the experimental results.

Compressor efficiencies are expected to be 50-70% for the isentropic efficiency and between 70% and 90% for the electrical efficiency. Problems arose from the compressor outlet temperature measurement. The measurement was reading too low a temperature and indicated an isentropic efficiency of greater than 90%. The working hypothesis for this is that the thermocouple is located too far from the true outlet of the compressor. Due to the heavy integration of the stack, the location of the thermocouple cannot be changed without compromising the performance of the stack. Therefore, isentropic efficiencies were chosen to fit the power consumption of the compressor rather than the outlet temperature.

The power consumed is the more important value in the model. Also, compressor efficiencies would be known to a designer using this model as an aid to system design. Electrical efficiencies are also chosen to match the model to the experimental data. The isentropic efficiency used for the compressor is 60% while the electrical efficiency is chosen to be 90%. For the Nexa system model, the only efficiency that really matters is the equivalent efficiency that encompasses both the isentropic and electrical efficiencies. In other words, the isentropic efficiency can be chosen to be higher if the electrical efficiency is chosen lower. However, in real world applications of this model, a designer has much better data on each of these efficiencies for the compressor in consideration for the system than is available for the Nexa system

A plot of experimental and modeled parasitic losses versus cathode air flow rate is found in Figure 24. For the upper half of the Nexa module's power range, the model overestimates the compressor power. This overestimation may be due to problems with the Nexa module reporting inaccurate values without the stack generating current. This suspicion arose because the reported parasitics of the stack do not agree with the Nexa documentation without the stack generating current. A better idea of the overall parasitic model validity is seen when total parasitics are analyzed with the stack running.

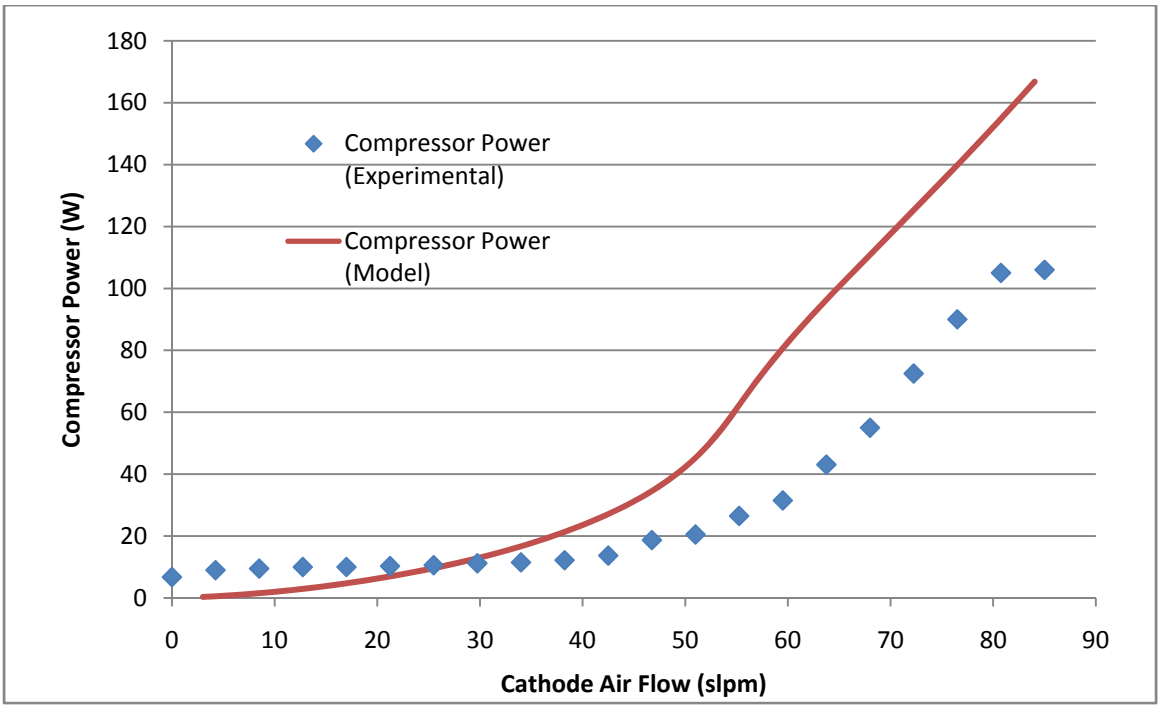

Figure 24. Compressor parasitics versus cathode flow rate

The cooling blower efficiency is modeled as a single efficiency in that the temperature rise due to compression is minimal and does not affect the model. Therefore, overall blower efficiencies are expected to be 50 – 75%. Like the compressor model, the blower efficiencies are chosen to match the model to the experimental parasitic data. The blower efficiency is chosen to be 70% based on experimental data. A plot of the blower parasitics is seen in Figure 25. For most of the operating range, the model overestimates the blower power. Like the compressor model, this may be a problem with the Nexa module not reporting accurate values with the stack not running. Looking at the overall parasitic model accuracy gives a better idea of the validity of the parasitic model.

The final step for fully validating the parasitics model is to compare the combined predicted model with experimental data from a running stack. A plot of these results is given in Figure 26. Because it is likely that the Nexa module does not report accurate data while not generating current the parasitic component efficiencies are chosen to best fit the overall parasitic losses. If the efficiencies were chosen to match the individual component data collected, the overall model losses would greatly underestimate the overall losses.

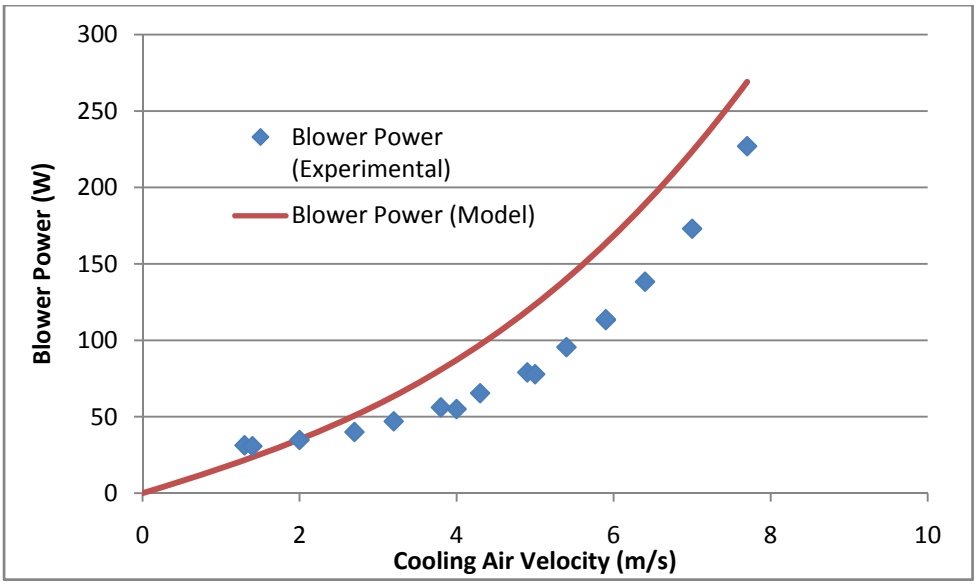

Figure 25. Blower parasitics versus cooling air speed

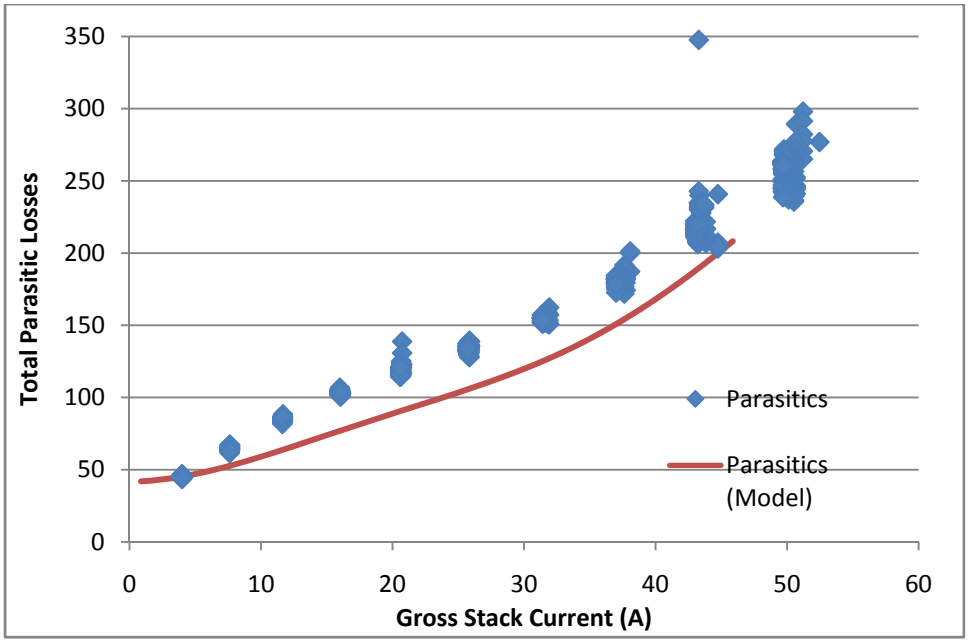

Figure 26. Total parasitic losses versus stack current

6. Example Model Results

Now that the model is fully validated, it can be used to better understand how fuel cell stack systems operate in conditions that may not be able to be simulated by real world testing or may pose too high of a risk for hardware damage. Two examples of this that will be evaluated in this thesis work are extreme heat and extreme cold.

Finally, the net system efficiency will be investigated with the model in typical operating temperatures with a ramping current demand.

6.1 Extreme Heat

Extreme heat situations on a fuel cell system can push the cooling system to its limits. Most fuel cell systems today are designed to operate at 80 °C. Anything above this temperature and the membranes start to break down causing permanent damage to the stack. Instead of risking expensive fuel cell hardware in high ambient temperature conditions, it is much safer and cost effective to do the testing with a validated model.

The Nexa fuel cell system is rated to operate in ambient temperatures of up to 40 °C. The control system in the Nexa module tries to keep the stack temperature at 60 °C. The maximum velocity that the blower can push the cooling air through the stack is known to be 7.7 m/s. With this, the worst case extreme heat scenario would be an ambient temperature of 40 °C, cooling fans working at maximum, and the stack operating at maximum gross current output of 45 A. When these conditions are put into the model, the maximum stack temperature is 76.65 °C. A plot of this simulated experiment is in Figure 27. The maximum temperature exceeds the desired temperature of the stack but is just below the maximum temperature for most PEMFCs. With this simulated data it is clear that the Ballard engineers specified the maximum ambient operating temperature to be this worst case scenario where the cooling system can keep the stack just below the 80 °C maximum PEMFC temperature.

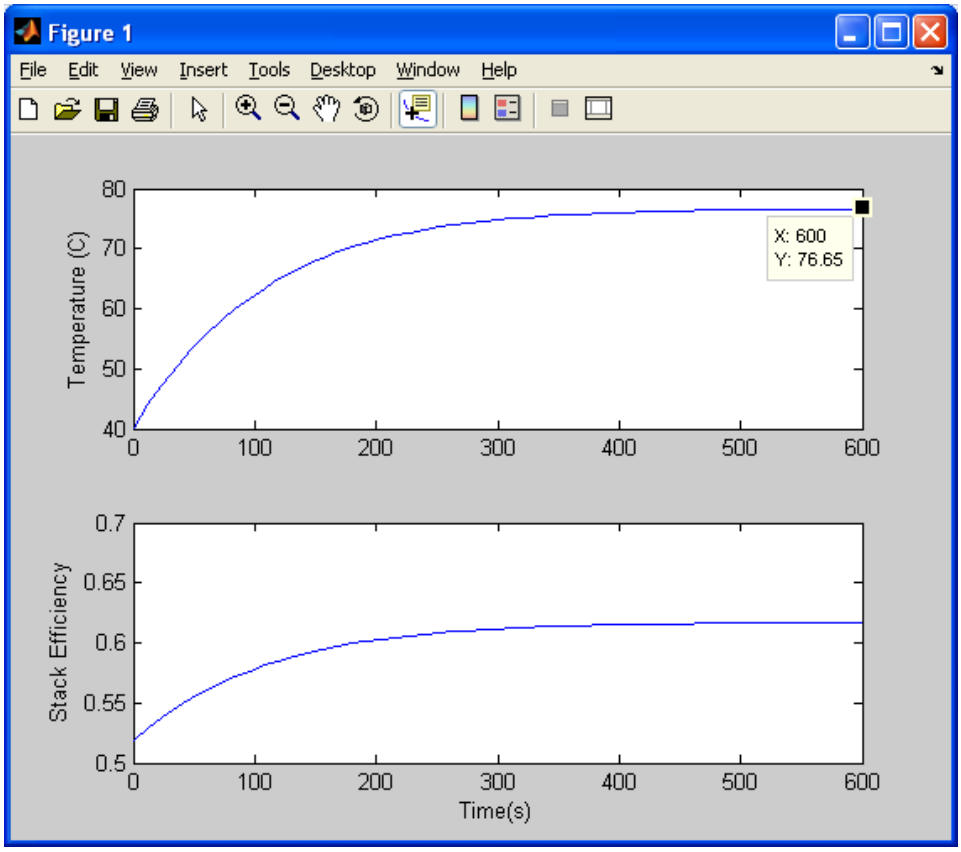

Figure 27. Extreme heat worst case scenario yields a maximum stack temperature of 76.65 °C

6.2 Extreme Cold

Fuel cells may have issues operating in temperatures below freezing because the membranes require liquid water to maintain their ion conductance. In addition, fuel cells will not work at full capacity at near freezing temperatures due to the cold hindering the electrochemical reactions. This lack of performance in cold ambient conditions is one of the key problems facing fuel cell engineers today. Mathematical models prove useful in understanding these cold weather conditions without sacrificing expensive hardware.

If the fuel cell is operating in an ambient temperature of 0 °C and has an initial temperature of 1 °C, what is the maximum power the fuel cell can produce and how long does it take to warm up? At these temperatures, the stack is going to be operating with the cooling fan at its lowest cooling air velocity of 2.1 m/s. Initially, the fuel cell can only produce around 1.1 kilowatts of gross power. Taking into account the parasitics, this is only 975 W net. That is 225 W less than the rated power of the stack. This power limitation with temperature is illustrated in Figure 28. It is clear that with time the available power in the stack increases. The stack reaches its rated power in approximately 250 seconds. This is due to the heating of the stack from the generated heat of the cathode electrochemical reaction. Rated power is reached when the stack reaches 45 °C.

Efficiency also suffers in cold conditions. The stack starts out at only a 40% efficiency not taking parasitics into consideration.

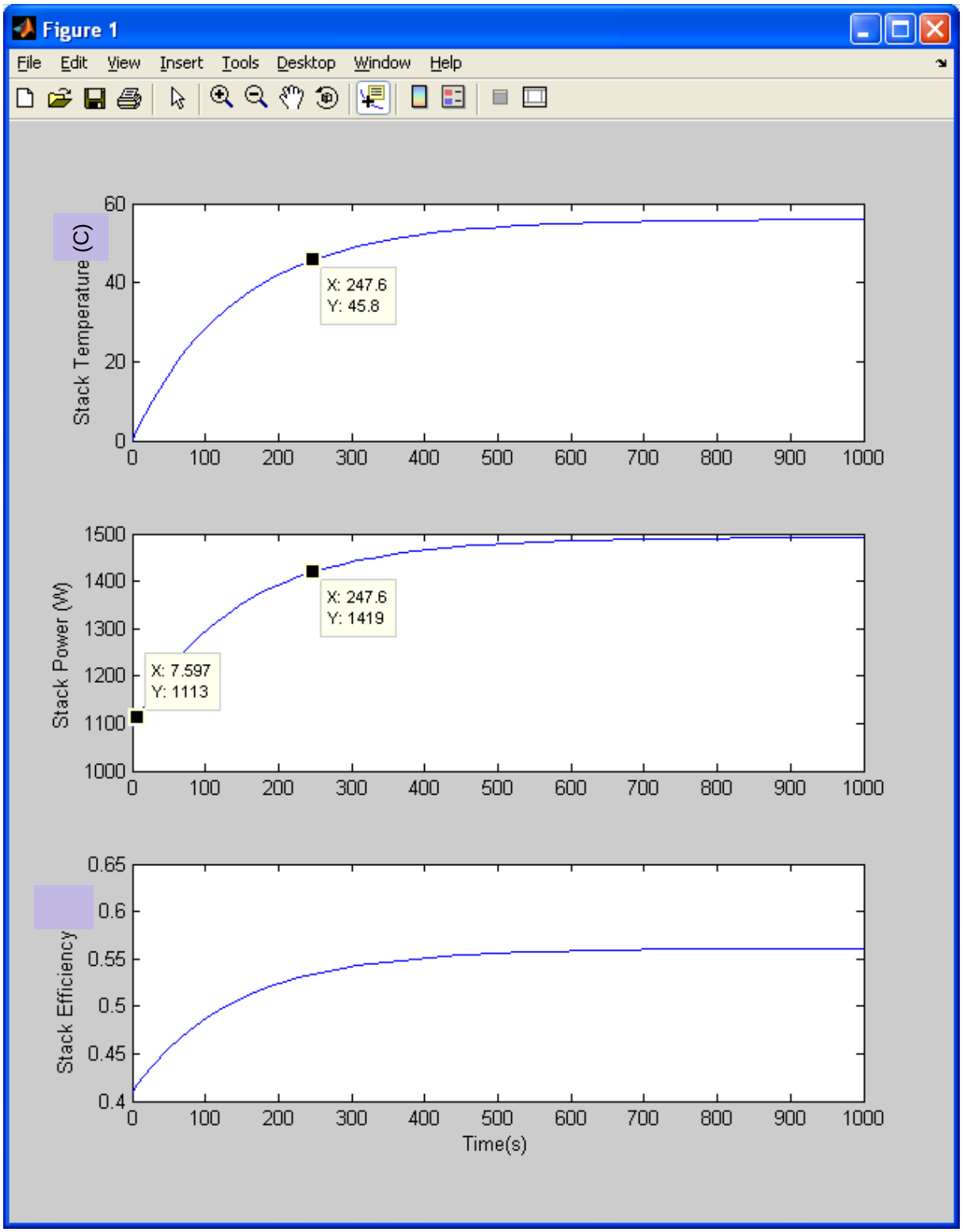

Figure 28. Extreme cold limits the power, and efficiency of the stack.

6.3 Net System Efficiency

Parasitic losses significantly influence the amount of usable power a fuel cell system can generate. Hydrogen fuel is consumed to generate the power that the parasitics use, but none of that power is usable by an outside system. Therefore, the more the parasitics of a system are reduced, the more efficient that system becomes. A comparison between the gross stack efficiency and the net system efficiency with respect to net current draw is shown in Figure 29. At low load, the system efficiency declines greatly. This is because the parasitics are a much larger proportion of the stack power at low loads than at high loads. It is also important to note that the system efficiencies actually start to increase at high loads. This is due to the increase in temperature that the stack experiences at high load. Other causes may be the increase in cathode air pressure and more reasonable oxygen stoichiometric ratios at higher loads. The temperature effects are further visible in Figures 27 and 28 and Table 12, while higher cathode air pressures and more reasonable oxygen stoichiometric ratios can be seen in Figure 19.

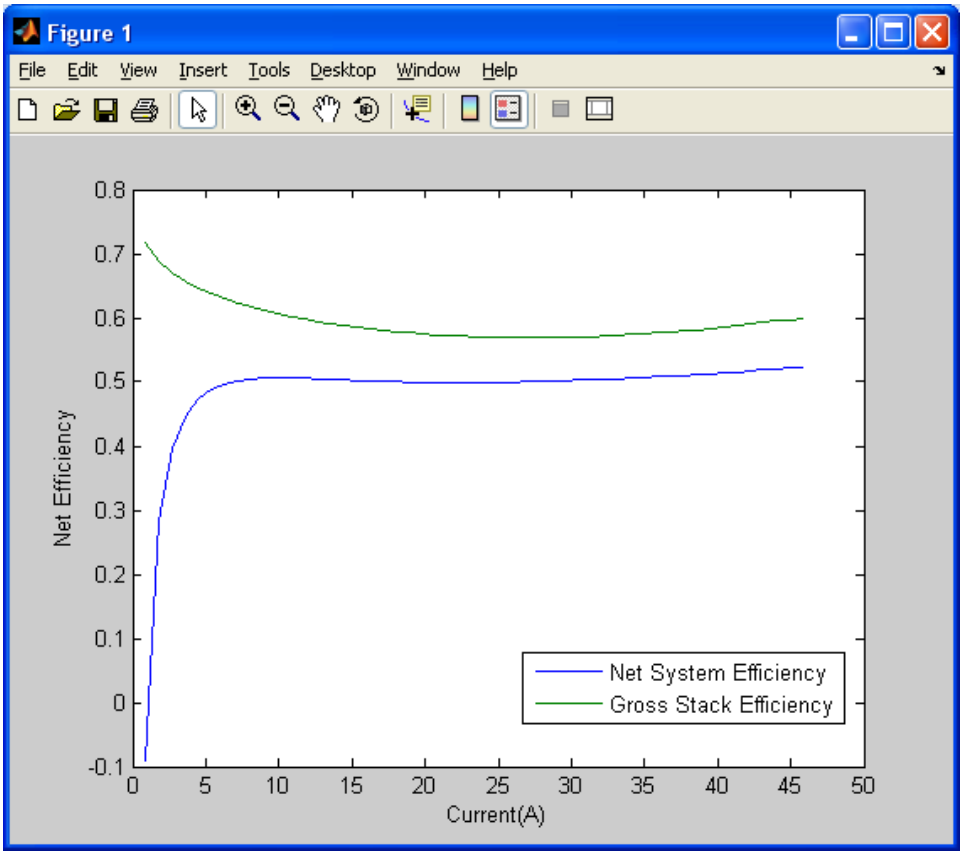

Figure 29. Comparison between stack and system efficiency

7. Future Research

The purpose of this research project was to develop a transient thermal model that allows for a system design engineer to evaluate different fuel cell hardware computationally. The key focus of this model is on the transient thermal properties of a stack. There were several setbacks to the development of this model due to funding and time limitations. These include the limitation of the model to air cooled stacks, the empirical polarization curve model, and limited validation resources for the parasitics and water management models.

If a water cooled stack were to become available in the future for validation, this model would benefit from the addition of a water cooled model. With this addition, the designer could better understand the benefits and drawbacks between an air cooled stack and a water cooled stack before any hardware was purchased. The water cooling stack would need to include a radiator cooling model, fan parasitic loss model, and a pump parasitic loss model. For large high power automotive stacks, water cooling is the obvious choice for the cooling system due to the space savings and need to remove large amounts of heat. Conversely, for smaller, low power stacks, air cooling would have the greater benefit due to the lower cost components and small amounts of heat that needs to be removed. The addition of a water cooling model would help in the decision between water cooling and air cooling for all of the stacks that fall in between these two categories where there is no clear choice.

If extra Nexa modules or even single cells became available, the model would benefit from a more detailed electrochemical model of the cells. Such a model was not possible with the hardware available due to the high level of integration of the fuel cell components. A more detailed electrical model would be based on the type of electrolyte membrane used, thickness of the membrane, humidification of the inlet gasses, distribution of catalyst at the reaction sites, GDL material and thickness, and many other parameters. Such a model could help cell designers understand how to better utilize platinum and other precious metal catalyst to their full potential to reduce the cost of stacks. Additionally, this kind of model would help understand different membrane materials that also may reduce stack costs. Many resources would be required for this model including access to different membrane, catalyst, and GDL materials.

Another area for expansion of this model is in the parasitic model section. The Nexa system provided poor parasitic data without the stack generating current. If a Nexa system that could be cannibalized for its compressor and blower became available, improvements could be made to the parasitic model. By connecting the blower and compressor to a separate power supply that could be easily monitored for voltage and current draw and incrementing the compressor with thermocouples in better locations, the parasitic components could be benchmarked for isentropic and electrical efficiencies. Unfortunately, a spare Nexa was not available to this project.

Like the parasitics model, the water management model would benefit from spare Nexa parts that could be characterized while not integrated into the Nexa system. A spare humidity exchanger with humidity and temperature transducers on all four ports would allow for both the thermal effectiveness and water vapor effectiveness to be characterized for a plethora of temperature and humidity scenarios. Data such as this could lead to a better humidity exchanger estimate than the simple one used in this model.

This transient thermal model provides a great resource for understanding the thermal properties of a virtual stack. This model still has room for expansion into many other aspects of a fuel cell system, or this model could be incorporated into an existing model that needs a validated transient thermal model.

8. Conclusions

This thesis work presents a transient thermal model of a PEMFC system. This model is a very useful tool to a fuel cell system design engineer to better understand a stack's characteristics and behaviors without needing the expensive hardware. This model is especially useful when investigating extreme ambient conditions that could permanently damage a stack. This model allows for these situations to be understood without needlessly risking expensive hardware experimenting in these conditions. For example, cold start conditions are one of the key limiting factors in the widespread emergence of fuel cells into the consumer market. Early in a stack's development, there is typically a limited amount of hardware available for testing. Engineers must plan for cold weather operating conditions but cannot risk the limited hardware in scenario's were it may be permanently damaged. The engineer can use this model in early development until additional hardware is available.

This thesis work also outlines the hardware and procedures needed to fully validate a fuel cell system model. Each sub-system on the Nexa module was mathematically modeled and validated using the on-board data collection as well as additional transducers added to the system. The sub-systems modeled include the cooling system including the stack thermal behavior, electrochemical reactions, fuel and air requirements and delivery, parasitics, and water management system. Additional validation hardware included a mass flow meter for the hydrogen supply line, pressure transducer for the compressor outlet pressure, thermocouples for stack temperatures, and a shunt resistor to measure gross current flow.

All of the research objectives are met with this project. An air cooled Nexa system was modeled with a focus on the transient thermal physics. This model was fully validated experimentally. While the majority of this thesis work focuses on the Nexa system, this model is fully scalable to a stack with any number of cells and any size cell. The scalability of the model was not investigated experimentally due to lack of hardware. Once the model was validated, the usefulness of the model was illustrated by investigating the system's reaction to extreme heat and cold ambient conditions. This model can now be expanded in the future to include features such as a water cooled model or be integrated into an existing model that needs a fully validated transient thermal model.

References

1. O'Hayre, Ryan, et.al. Fuel Cell Fundamentals. New York: John Wiley and Sons, 2006.

3. United States Department of Energy. "Technical Plan - Storage." Multi Year Research, Development and Demonstration Plan. Washington DC, 2007. 3.3-1 - 3.3-22.

2.Pivovar, Bryan, et al. Sub-Freezing Fuel Cell Effects. FY 2005 Progress Report. Los Alamos, NM: Los Alamos National Laboratories, 2005.

4. "Ford Delivers Hydrogen Focus Fuel Cell Fleet." Motor Trend 28 October 2005.

5. Ougarov, Kirill. "GM launches hydrogen fuel-cell vehicle "Project Driveway" vehicle test." Motor Trend 18 October 2007.

6. HydrogenTrade.com. 10 January 2007 <http://www.hydrogentrade.com/fuel-cells/>.

7. California Fuel Cell Partnership. October 2007. 10 January 2007 <http://www.cafcp.org/fuel-vehl_map.html>.

8. Baschuk, J.J. and Xianguo Li. "A general formulation for a mathematical PEM fuel cell model." Journal of Power Sources (2004): 134-153.

9. del Real, Alejandro J., Alicia Arce and Carlos Bordons. "Development and experimental validation of." Journal of Power Sources (2007): 310-324.

10. Lee, J.H. and T.R. Lalk. "Modeling fuel cell stack systems." Journal of Power Sources (1998): 229-241.

11. Rowe, Andrew and Xianguo Li. "Mathematical modeling of proton exchange membrane fuel cells." Journal of Power Sources (2001): 82-96.

12. Incropera, Frank P. and David P. DeWitt. Fundamentals of Heat and Mass Transfer. Fifth Ed. Hoboken, NJ: Wiley, 2002.

13. Shevock, Bryan and Jonathan Schoenfeld. Automotive ConSERV System Applications . Washington DC: United States Department of Energy, 2005.

14. Haraldsson, Kristina and Keith Wipke. "Evaluating PEM fuel cell system models" Journal of Power Sources (2003): 88-97.

15. Gurski, Stephen. Cold Start Effects on Performance and Efficiency for Vehicle Fuel Cell Systems. Thesis. Virginia Polytechnic Institute and State University, Blacksburg, VA, 2002. ETDs @ VT. Scholar. Virginia Polytechnic Institute and State University Digital Library and Archives. 15 Oct. 2006 <http://scholar.lib.vt.edu/theses/>

Appendix A: Matlab .m File Code

Convective Cooling

```
%splitting the rectangular channels into two banks of fins

function Q = convective(B,l,w,t,N,Um,k,Tstack,Tamb,Ncells)

%B = 0.125603;
%l = 0.0030988;
%w = 0.0042926;
%t = 0.0020828;
%N = 18;
%Um = 2.2;
%k = 21;
%Tstack = 295.69;
%Tamb = 289.5;
%Ncells = 47;

%Constants
mu_air = 184.6e-7;
rho_air = 1.1614;
nu_air = 15.89e-6;
alpha_air = 22.5e-6;
k_air = 26.3e-3;
cp_air = 1007; %J/kg

%Convective cooling area of one plate and one fin
At = N*2*(l/2)*B + (N*w)*B;
Af = 2*(l/2)*B;

%Calculate Reynolds Number
Ac = l*w;
P = 2*l+2*w;
Dh = (4*Ac)/P;

Re = (rho_air*Um*Dh)/mu_air;

%Calculate Nusselt Number
f = (0.790*log(Re)-1.64)^-2;
Pr = nu_air/alpha_air;

if Re < 3000
    Nu = 3.068;
else
    Nu = ((f/8)*(Re-1000)*Pr)/(1+12.7*(f/8)^(1/2)*(Pr^(2/3)-1));
end

%Calculate convective heat transfer coefficient
h = (Nu*k_air)/Dh;

%Calculate fin efficiency
Pf = 2*(t+B);
```

```
Acf = t*B;
m = ((h*Pf)/(k*Acf))^(1/2);

nf = tanh(m*(l/2))/(m*(l/2));

%Calculate fin array efficiency
n0 = 1-((N*Af)/At)*(1-nf);

%Calculate log mean temperature difference

mdot = rho_air*Um*Ac;

Tout = Tstack-(Tstack-Tamb)*exp(-(2*n0*h*At)/(mdot*cp_air));

dTlm = ((Tstack-Tout)-(Tstack-Tamb)) / log((Tstack-Tout)/(Tstack-Tamb));


%Calculate q for one plate
q = 2*h*At*n0*dTlm;

%Calculate Q for the Stack
Qconv = Ncells*q;


%*********************************************************************
%Calculate convective heat transfer using a full channel model

To = Tstack-(Tstack-Tamb)*exp(-(P*B*h)/(mdot*cp_air));
Tlm = ((Tstack-To)-(Tstack-Tamb))/log((Tstack-To)/(Tstack-Tamb));

q_singch = h*P*B*Tlm;

Qtot = Ncells*N*q_singch;

Q = [Qconv,Qtot,To];
```

Humidity Exchanger

```
%Humidity Exchanger Model

function hum = HX(Elatent, Esense, Tcomp, Tstack, mdotO2out,
mdotN2out,mdotH20vout,wamb, mdotairin)

%Constants
c_air = 1007; %kJ/kg*K
cp_O2 = 920;
cp_N2 = 1041;

%Sensible Heat Model
q = Esense*(cp_O2*mdotO2out+cp_N2*mdotN2out)*(Tstack-Tcomp);
```

```
T2 = Tcomp-(-q/c_air);

Texhaust = Tstack-(q/(cp_O2*mdotO2out+cp_N2*mdotN2out));

%Latent HX model
% Elatent = (w wet in-w wet out)/(w wet in-wdry in)

mdottrans =
(mdotO2out+mdotN2out)*Elatent*((mdotH20vout/(mdotO2out+mdotN2out))-wamb);

mdotH2Oin = mdottrans+wamb*mdotairin;

hum = [T2, mdotH2Oin,Texhaust];
```

Parasitic Losses

```
%Calculate Parasitic losses

function Ploss =
parasitics(Eisen,Eel,mdotair,Pout,Tamb,Ebl,v,w,l,N,Ncells,Dcomp,h,Tcoolout,Qc
onv)

%Eisen = 0.6;
%Eel = 0.8;
%mdotair = 2e-3;
%Pout = 8;
%Tamb = 298;
%Ebl = 0.5;
%v = 2.2;
%w = 0.0042926;
%l = 0.0030988;
%N = 18;
%Ncells = 47;
%Dcomp = 0.009525;
%h = 0.125603;
%Tcoolout = 305;
%Qconv = 150;

%Constants
rho_air = 1.1614;
k = 1.4;
cp_air = 1007; %J/kg*K
Patm = 101.325;
R_air = .2870;
gamma_air = 11.43; %N/m^3
g = 9.81;
cv_air = 718;
mu_air = 1.846e-7;

%Compressor Losses

T2s = (((Pout+Patm)/Patm)^((k-1)/k))*Tamb;
```

```
T2 = ((T2s-Tamb)/Eisen)+Tamb;

Vcomp = mdotair/(rho_air*((pi*Dcomp^2)/4));

Pcomp = mdotair*(cp_air*(T2-Tamb)+(Vcomp^2)/2)/Eel;

%Blower Losses
%Pressure Required to blow through channel with known outlet velocity
Ac = l*w;
P = 2*l+2*w;
Dh = (4*Ac)/P;

Re = (rho_air*v*Dh)/mu_air;

f = (0.790*log(Re)-1.64)^-2;

dP = gamma_air*h + f*(h/Dh)*(v^2/(2*g));

mdotcool = rho_air*v*l*w*N*Ncells;

%blower calcs based on compressor equations
Tbs = Tamb*((dP+Patm)/Patm)^((k-1)/k);

rho_in = (Patm+dP)/(R_air*Tamb);
rho_out = (Patm)/(R_air*Tbs);

%Energy Equation
PbldT = mdotcool*(cv_air*(Tbs-Tamb));
PbldP = mdotcool*(((Patm+dP)/rho_in)-(Patm/rho_out));
PblV = mdotcool*((v^2)/2);
Pblower = (PbldT+PbldP+PblV)/Ebl;
%Pblower = Ebl*(mdotcool*(-(Patm/rho_in)+((Patm+dP)/rho_in)+(v^2/2)+g*h));

Ploss = [Pcomp,T2,Pblower];
```

Power and Efficiency Calculations

```
%Compute fuel cell power, efficiency, and qgen

function O = power_efficiency(I,V,mdotH2in)

LHV_H2 = 120100; %kJ/kg

%Compute Power
P = V*I; %W

%Compute qgen and efficiency
Pfuel = mdotH2in*LHV_H2*1000; %W
qgen = Pfuel-P; %W
E = P/Pfuel; % %
```

```
%Combine to a single vector
O = [P E qgen];
```

Vapor Test

```
%Determine if possible H2O vapor is greater than H20 out

function mdotH2O = vaportest(mdotH2Ovposs,mdotH2Oout)

if mdotH2Ovposs > mdotH2Oout
    mdotH2Ovout = mdotH2Oout;
    mdotH2Olout = 0;
else mdotH2Ovout = mdotH2Ovposs;
    mdotH2Olout = mdotH2Oout-mdotH2Ovout;
end

mdotH2O = [mdotH2Ovout, mdotH2Olout];
```

Appendix B: Simulink Code

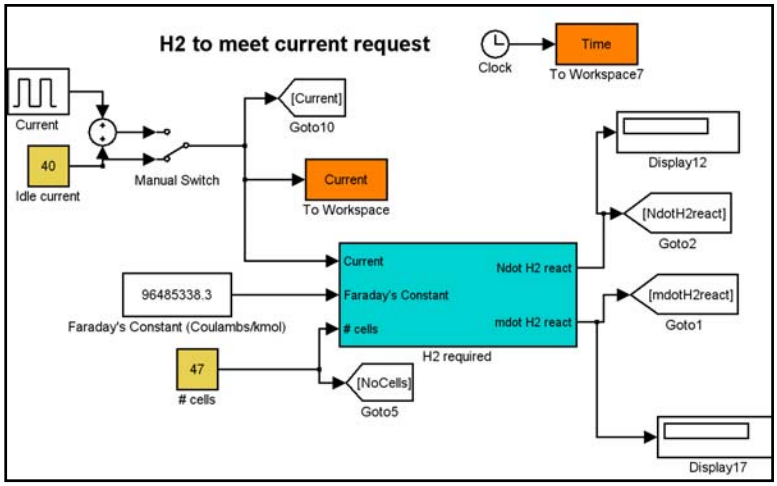

Figure B-1. Hydrogen to meet current request Simulink diagram

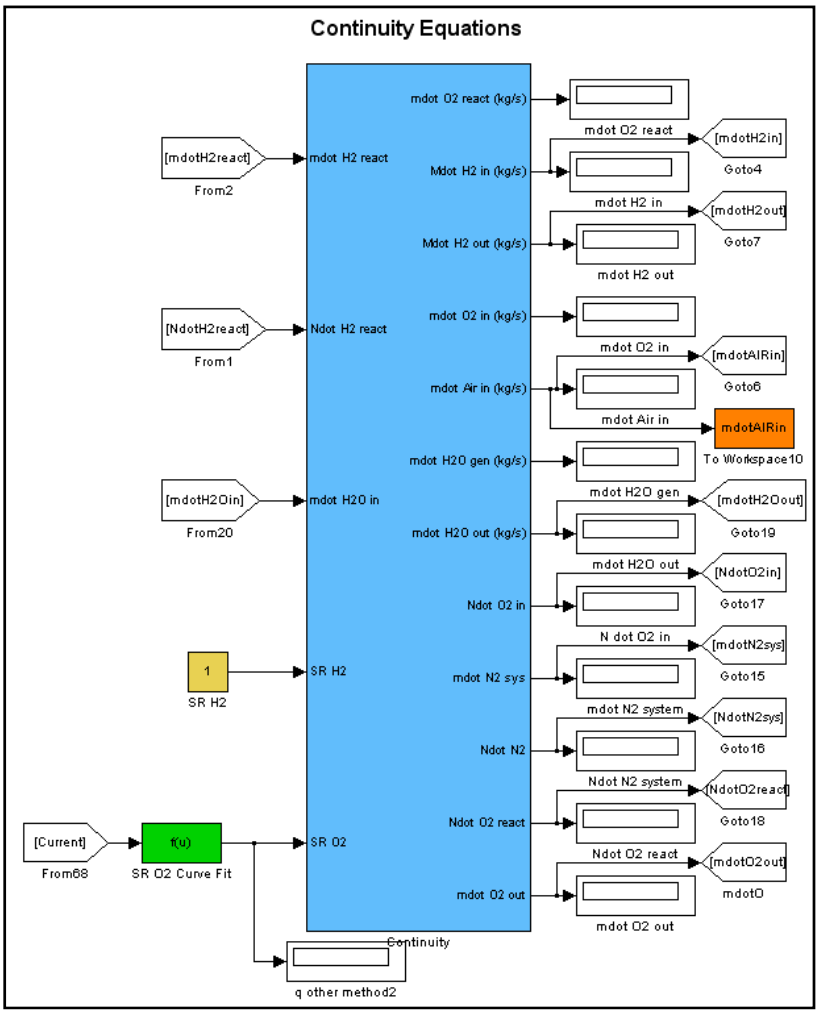

Figure B-2. Conservation of Mass Simulink Diagram

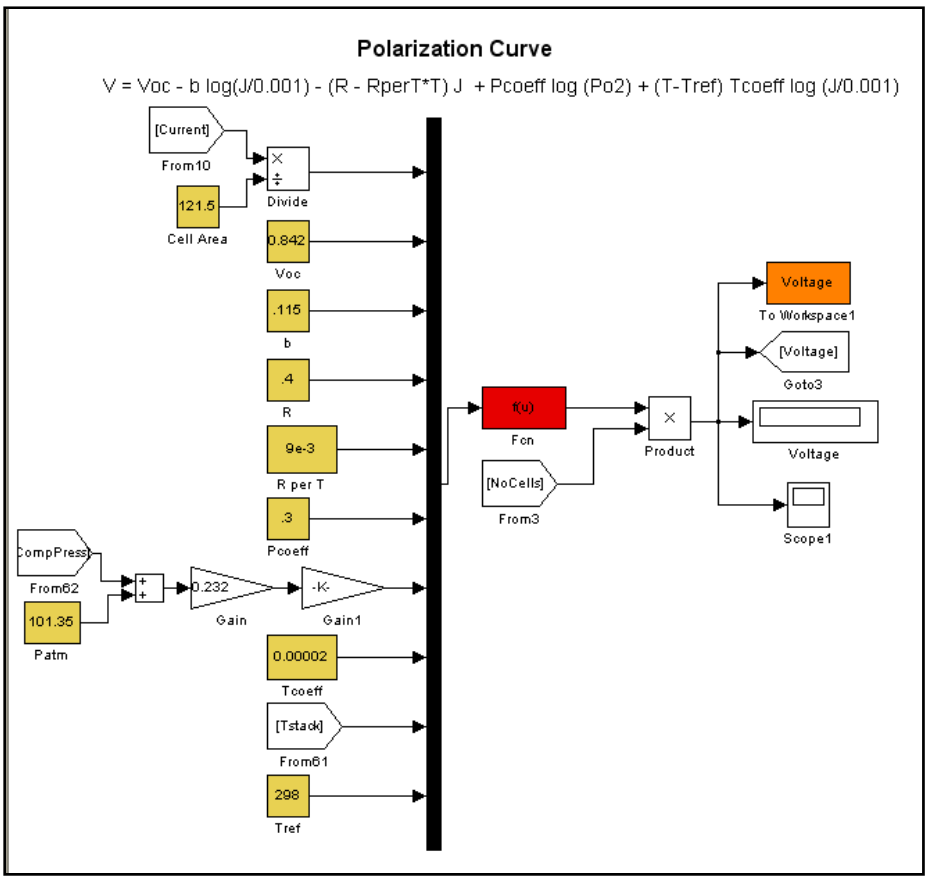

Figure B-3. Polarization Curve Simulink Diagram

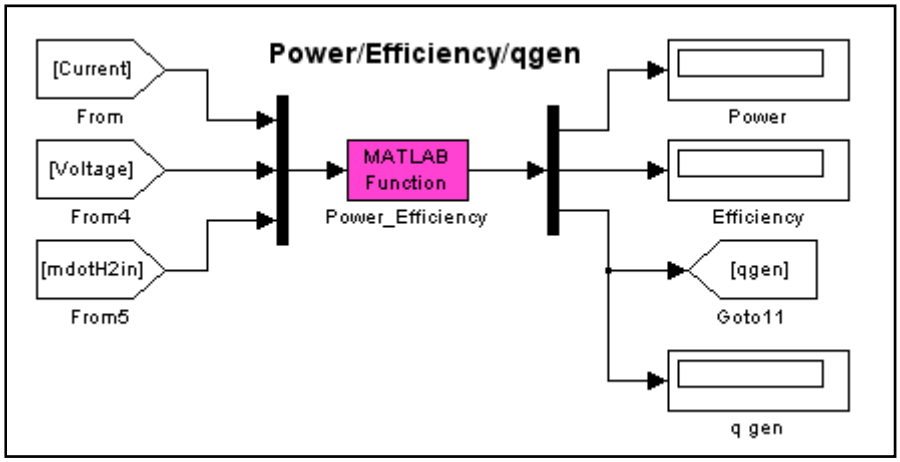

Figure B-4. Power/Efficiency/Heat generation Simulink Diagram

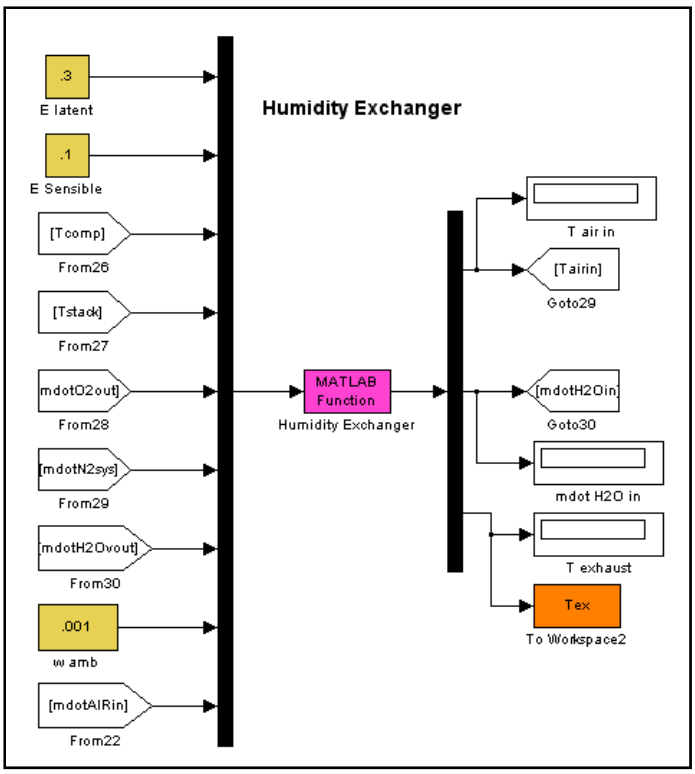

Figure B-5. Humidity Exchanger Simulink Diagram

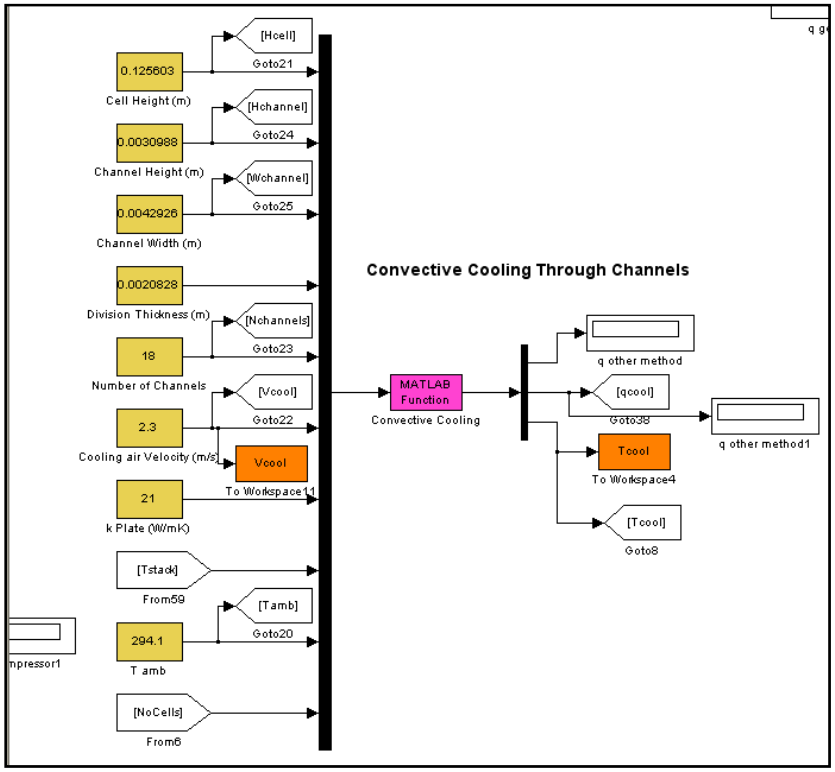

Figure B-6. Convective cooling Simulink Diagram

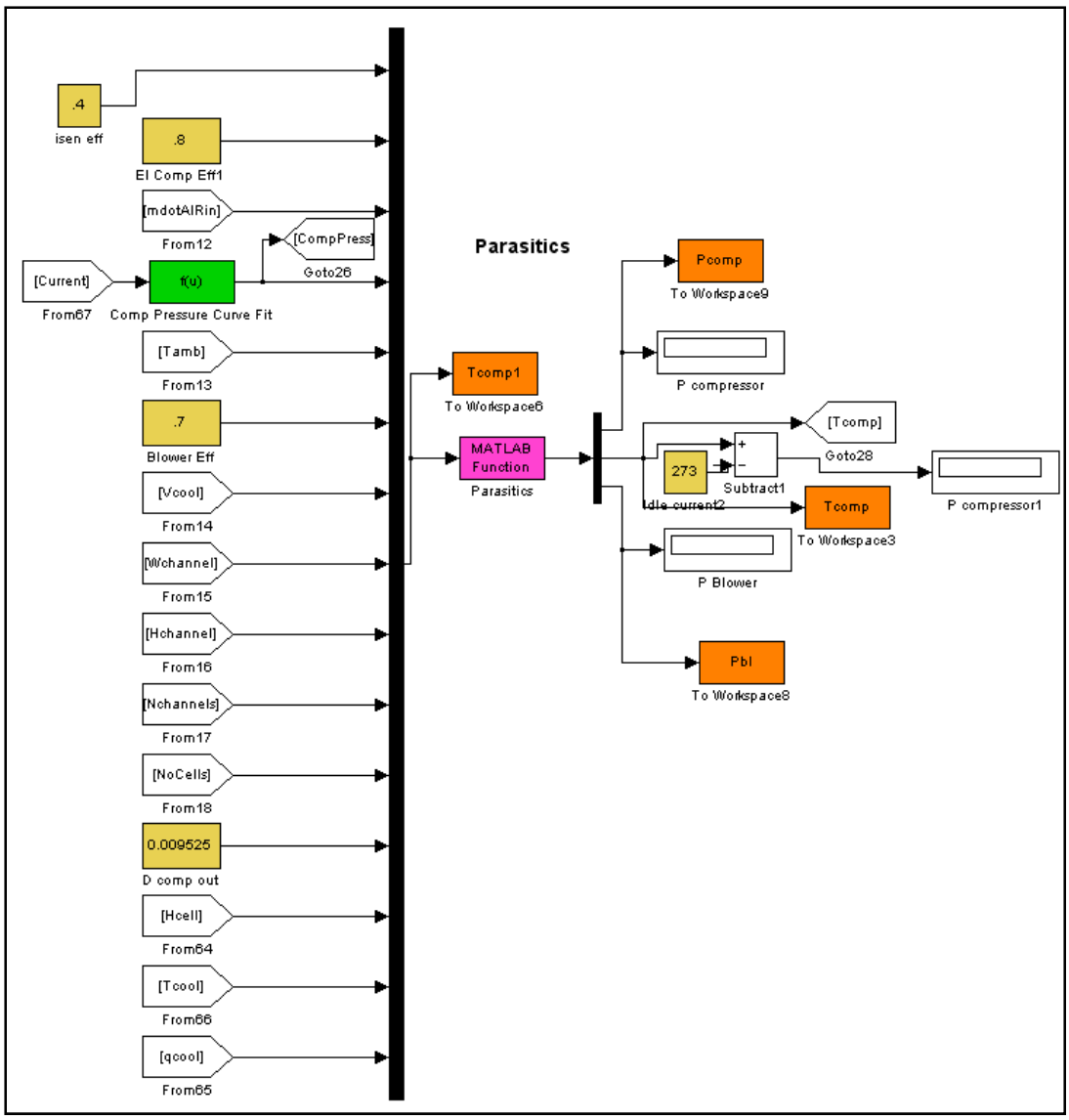

Figure B-7. Parasitics Simulink Diagram

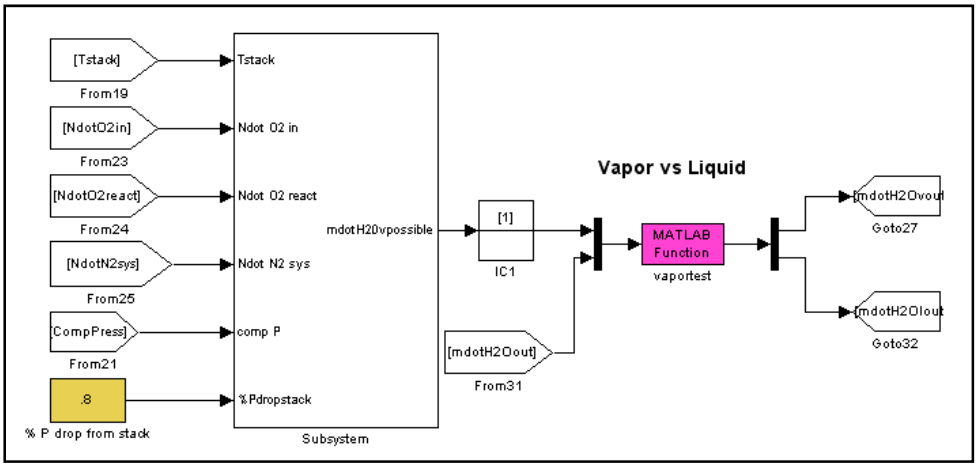

Figure B-8. Liquid and vapor outlet water calculation Simulink Diagram

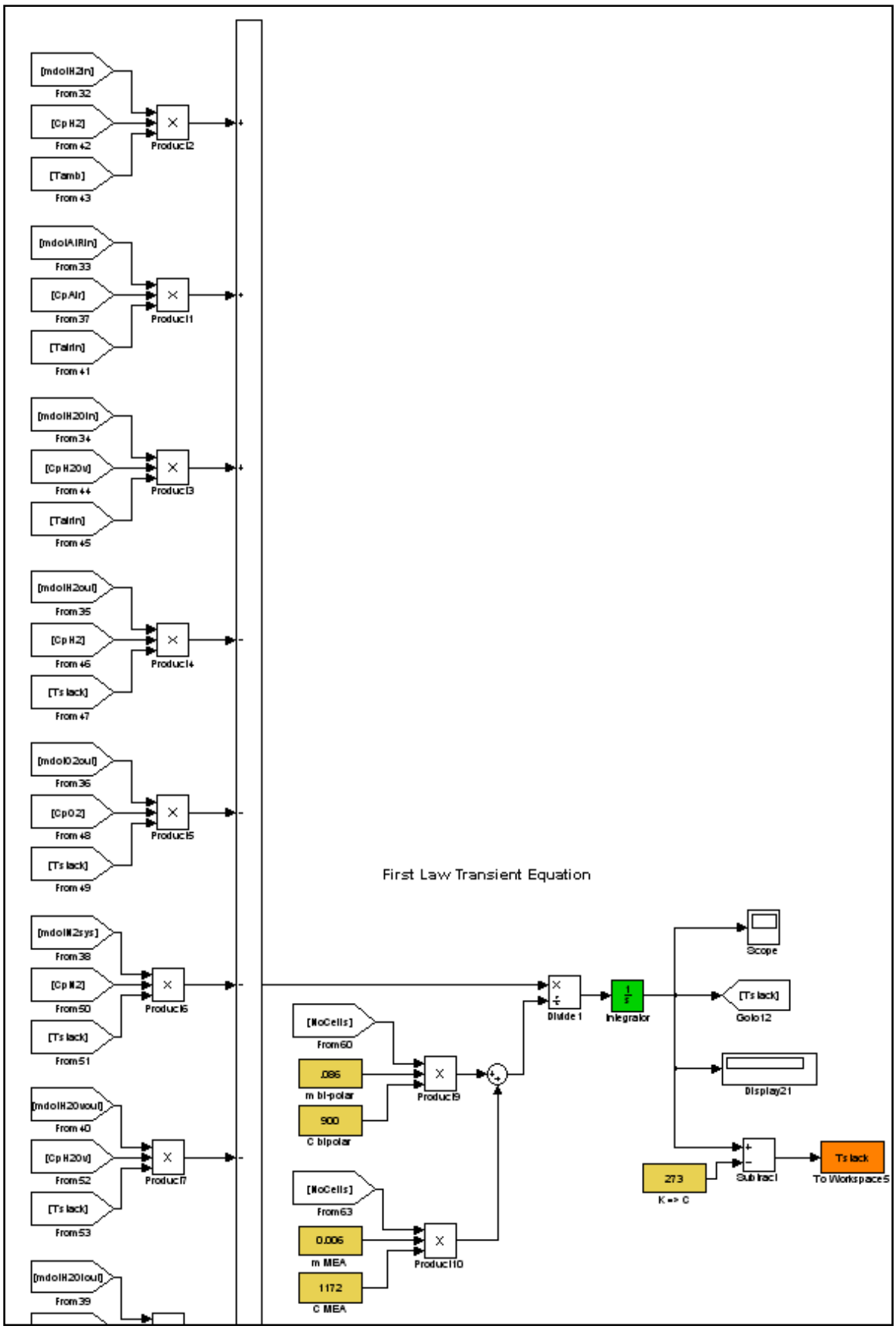
[mdotH2in]
From32
[Cp H2]
From42
[Tamb]
From43
Product2
[mdotAIRin]
From33
[Cp Air]
From37
[Tairin]
From41
Product1
[mdotH2Oin]
From34
[Cp H2Ov]
From44
[Tairin]
From45
Product3
[mdotH2out]
From35
[Cp H2]
From46
[Ts lack]
From47
Product4
[mdotO2out]
From36
[Cp O2]
From48
[Ts lack]
From49
Product5
[mdotN2sys]
From38
[Cp N2]
From50
[Ts lack]
From51
Product6
[mdotH2Ovout]
From40
[Cp H2Ov]
From52
[Ts lack]
From53
Product7
[mdotH2Olout]
From39
First Law Transient Equation
[NoCells]
From60
.086
m bi-polar
900
C bipolar
Product9
[NoCells]
From63
0.006
m MEA
1172
C MEA
Product10
Divide1
Integrator
Scope
[Ts lack]
Goto12
Display21
273
K => C
Subtract
Ts lack
To Workspace5

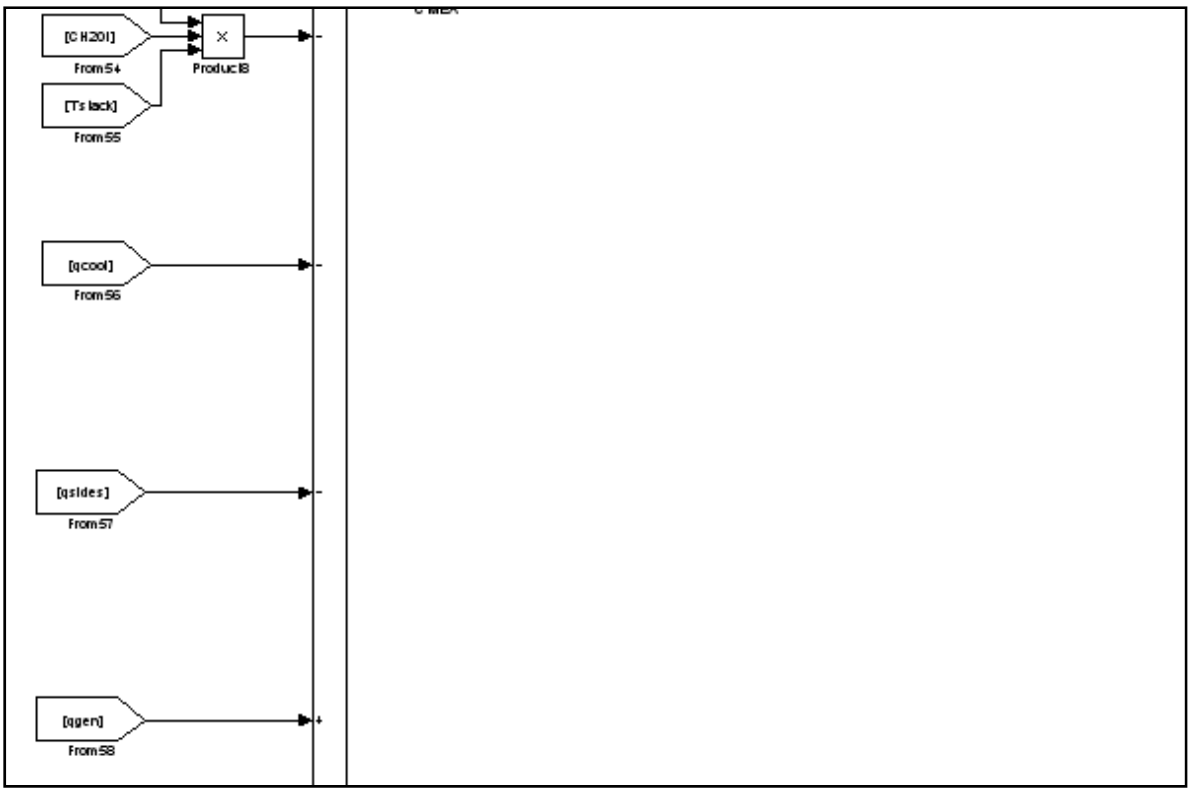

Figure B-9. Transient Thermal Model Simulink Diagram

Vitae

Bryan W. Shevock

Contact:
bshevock@vt.edu

EDUCATION

B.S. Mechanical Engineering, May 2006
Virginia Tech, Blacksburg, VA
Overall GPA: 3.35 / 4.0

M.S. Mechanical Engineering, Expected Graduation Spring 2008
Virginia Tech, Blacksburg, VA
Overall GPA: 3.51 / 4.0

WORK EXPERIENCE

Hybrid Vehicle Integration Engineer, General Motors, Milford, MI
Since February 2008

- Energy and Drive Quality Engineer

Summer Engineering Internship, General Motors, Milford, MI
Summer 2007

- Managed Energy storage system hardware for a development fleet of hybrid vehicles

Summer Engineering Internship, Ford Motor Company, Dearborn, MI
Summer 2006

- Designed a new concept for battery module assembly into a high voltage battery pack for NiMH and Li-ion applications and submitted the design for patent.
- Adapted advanced welding techniques for use in Lithium-Ion cell welding processes.

Summer Engineering Internship, Sandia National Laboratories, Livermore, CA.
Summer 2004

- Conducted experiments and analyzed data to develop advanced hydrogen storage materials.
- Created several analysis programs to analyze stress and thermal properties of several hydrogen storage systems.

Summer Engineering Internship, Sentech Inc, Department of Energy Headquarters, Washington, DC.
Summer 2005

- Created a computer model to explore HVAC load reduction techniques to improve fuel economy.

RELATED SCHOOL EXPERIENCE

Graduate Research, Virginia Tech, Blacksburg, VA
Fall Semester 2006 – Fall Semester 2007

- Developing a system level transient thermal computer model of a Hydrogen PEM fuel cell stack.
- Validating the model with an instrumented Ballard Nexa fuel cell system.

Hybrid Electric Vehicle Team Mechanical Team Leader, Virginia Tech, Blacksburg. VA
2005-2006 Academic Year

- Organized groups and conducted other administrative duties.

Senior Design Project Group Leader, Virginia Tech, Blacksburg, VA.
2005-2006 Academic Year

- 12 Volt/ High Voltage Accessory team leader for the Hybrid Electric Vehicle Team (HEVT) competing and winning First Place Overall in the 2006 Challenge X competition.
- Designed and integrated the 12V system and new electrical accessories to replace previously belt driven systems including the air conditioning compressor and alternator.

Undergraduate Research, Virginia Tech, Blacksburg, VA.
Spring Semester 2005

- Designed a hydrogen fuel cell auxiliary power unit for HEVT.
- Petitioned for and obtained sponsorship from companies to provide costly parts.

Undergraduate Research, Virginia Tech, Blacksburg, VA.
Fall Semester 2004

- Researched battery discharge characteristics through experimentation for HEVT.

COMPUTER SKILLS

Matlab	AutoCAD	Minitab
Simulink	Inventor	MS Excel
LabVIEW	FEMLAB	MS Word
NX3 (Unigraphics)	Mathcad	MS PowerPoint
Pro/ENGINEER	Mathematica	

ACTIVITIES AND HONORS

Published SAE paper #2008-01-0636 “System Level Transient Model of a Fuel Cell System
National Society of Collegiate Scholars, member, 2003 – present
Hybrid Electric Vehicle Team of Virginia Tech, member, 2004 – present
University Honors Program, 2002 - 2003
Pamplin Leader, 2002 – 2003